Research Square

Preprints are preliminary reports that have not undergone peer review.
They should not be considered conclusive, used to inform clinical practice,
or referenced by the media as validated information.

Mapping Recovery After Hurricane Katrina, 2004-2025: A Multi-Temporal Machine Learning and Trajectory-Based Analysis of Greater New Orleans

Stanley Osondu

stanley.osondu@utdallas.edu

The University of Texas at Dallas https://orcid.org/0009-0006-8717-5920

Muhammad Tauhidur Rahman

The University of Texas at Dallas https://orcid.org/0000-0003-1348-0536

Research Article

Keywords: Hurricane Katrina, Disaster recovery, Land cover change, Remote sensing, Machine learning, Spatial autocorrelation

Posted Date: November 3rd, 2026

DOI: https://doi.org/10.21203/rs.3.rs-11576870/v1

License: This work is licensed under a Creative Commons Attribution 4.0 International License.
Read Full License

Additional Declarations: The authors declare no competing interests.

Title: Mapping Recovery After Hurricane Katrina, 2004-2025: A Multi-Temporal Machine Learning and Trajectory-Based Analysis of Greater New Orleans

Article type: Original Paper

Authors: Stanley Ejike Osondu[1] [0009-0006-8717-5920] · Muhammad Tauhidur Rahman[2] [0000-0003-1348-0536]

[1,2] Geospatial Information Science, University of Texas at Dallas, Richardson, Texas, 75080, United States

Corresponding author: Stanley Ejike Osondu - stanley.osondu@utdallas.edu

Abstract

Hurricane Katrina (2005) and the subsequent levee failures caused one of the largest urban disasters in U.S. history. However, the spatial extent, timing, and environmental consequences of rebuilding across the Greater New Orleans region remain poorly quantified at the metropolitan scale. This study maps land cover for seven epochs (2004–2025) using Landsat 5, Landsat 8, and Sentinel-2 imagery. Four machine learning classifiers (Random Forest, Extreme Gradient Boosting (XGBoost), Support Vector Machine, and K-Nearest Neighbors) were trained on a 20-feature spectral stack and evaluated using spatial-split cross-validation, yielding overall accuracies of over 90%. XGBoost performed comparably to the other classifiers and was used to produce the final maps. SHAP analysis showed that the spectral features driving classification shifted across epochs, with the blue band dominating in 2005 (consistent with post-flood standing water). Pixels were grouped into seven change trajectories. The largest, “Decline then Recovery” (built-up in 2004, non-built-up after the storm, and built-up again by 2013 or later), covered 97.88 km², compared with 1.96 km² for “Built-up Loss” (built-up before the storm and never recovered).

Global Moran's I showed significant spatial clustering across all trajectories (I = 0.14–0.55, $p < 0.001$). Local Indicators of Spatial Association (LISA) identified 39 tracts with high recovery shares surrounded by similar tracts, and 62 tracts with low recovery shares surrounded by similar tracts (mainly in the Lower Ninth Ward and New Orleans East). Overall, post-Katrina recovery has been extensive but spatially uneven, with some neighborhoods rebuilt and others still lagging.
Keywords: Hurricane Katrina; Disaster recovery; Land cover change; Remote sensing; Machine learning; Spatial autocorrelation.

Highlights

- Longest continuous satellite record (2004–2025) of a single US disaster recovery
- Built-up recovery (97.9 km²) far outweighs permanent loss (2.0 km²) region-wide
- Recovery clusters in elevated, affluent areas; Lower Ninth Ward remains a cold spot
- 92.8% of new development (124 km²) converted forested wetland to impervious surface
- SHAP shows floodwater signatures, then wetland regrowth, driving classifier decisions

1. Introduction

Hurricane Katrina and the August 29, 2005 levee failures created one of the most significant urban shock events in US history by displacing over 1 million people along the Gulf Coast and damaging much of New Orleans' housing stock and infrastructure (Kates et al. 2006; Fussell 2015). The storm also exposed long-standing vulnerabilities in the region's physical environment, in racialized patterns of urban development, and in socioeconomic inequality (Gotham and Campanella 2011; Scoppetta 2016). Because rebuilding decides where people and assets will be located when the next storm arrives, recovery is not only a social process but a central part of long-term risk hazard. It determines whether exposure is reduced, restored to its previous level, or increased.

The social-science literature has documented that recovery after Katrina was highly uneven. Neighborhoods with higher pre-storm property values and income levels returned to residential use faster than low-income neighborhoods primarily populated by Black residents (Kamel 2012; Fussell 2015). Federal relief and property-transfer programs often reinforced earlier disparities, and the most heavily damaged neighborhoods received comparatively little funding and post-disaster real-estate investment (Kamel 2012; Kondo 2017a). Market-oriented redevelopment (Gotham and Greenberg 2008; Scoppetta 2016) and "climate gentrification" of higher-elevation neighborhoods less affected by flooding (van Holm and Wyczalkowski 2018; Aune et al. 2020) further concentrated investment where flood exposure was lowest. Elevation, flooding, and recovery are therefore linked, and the spatial pattern of rebuilding is a question of hazard exposure as much as of social equity.

Satellite remote sensing is widely used to map hurricanes and flood impacts and to monitor post-disaster change over large areas. However, studies of long-term recovery after Katrina, have

mostly relied on a few time points, administrative records, or neighborhood case studies, which cannot capture how recovery unfolded across a whole metropolitan area (Fussell 2015; Chuang et al. 2019; Wang et al. 2025). Satellite studies of post-Katrina urban change have generally used binary built-up/non-built-up change detection with two or three dates (Qiang and Lam 2016), and so do not follow pixels through the full sequence of pre-storm, flooded, and recovered states. Machine learning has been applied to post-disaster redevelopment (Lin et al. 2024), but the applications of combining a multi-sensor record in the New Orleans coastal deltaic setting is lacking. Furthermore, very few remote-sensing recovery studies have examined whether observed spatial patterns are statistically non-random (i.e. with spatial autocorrelation statistics (Anselin, 1995)), or explain which spectral features drive classification decisions at each stage of recovery (Lundberg and Lee 2017). This study addresses these gaps.

The objective of this study is to examine land cover change in Greater New Orleans over seven dates between 2004 and 2025, spanning the pre-Katrina baseline, the immediate post-storm state, and two decades of recovery. To do so, multi-sensor land cover classification, SHAP-based interpretation, pixel-level trajectory analysis, spatial autocorrelation (Global Moran's I and Local Indicators of Spatial Association, LISA), and tract-level clustering analysis have been combined. More specifically, the research objectives are to: (1) produce accurate land cover maps for all seven dates, and use SHAP analysis to identify which spectral features drive classification at each stage of the recovery; (2) quantify how much built-up land was lost after Katrina and how much returned, using pixel-level change trajectories; (3) examine whether patterns of recovery and non-recovery are spatially clustered, using Global Moran's I and Local Indicators of Spatial Association (LISA); and (4) group census tracts into neighborhood types based on trajectory composition, elevation,

and infrastructure measures. The results will highlight areas where rebuilding occurred, how extensive it was, and what it implies for future flood exposure.

2. Study Area

The research area covers five parishes of the Greater New Orleans metropolitan area in south-eastern Louisiana: Orleans, Jefferson, St. Bernard, Plaquemines & St. Charles (Figure 1). Together, they cover almost 630 km², encompassing much of the lower Mississippi River Delta – a submerging coastal floodplain that is primarily located beneath mean sea level and features a varied mix of urban areas, wetland forests, emergent marshes, and open waters. This unique combination of features means this region is particularly susceptible to effects from hurricanes and at the same time presents substantial challenges when using remote sensing techniques to identify different types of land use.

Before Katrina, the 5-parish study area contained a population of around 1 million residents (2000 census), and Orleans parish included 485,000; the population of New Orleans alone was about 455,000 just before the hurricane. A comparison of the race-based demographics of the study area revealed considerable variation among parishes; at the time of the 2000 census, Orleans Parish was 67% black and 28% white. It made it one of the most predominantly black large cities in the country. In contrast, Jefferson, St. Charles, and Plaquemines parishes were all predominantly white. Following Katrina, the Black population of New Orleans declined by almost 60 percent, and the white population dropped by approximately 35%; however, the city of New Orleans remains a minority-majority city with approximately 59% of the remaining population being Black. Immediately after Katrina, the overall population of the city of New Orleans dropped by more than half from 455,000 to less than 235,000.

Although only slightly smaller, St. Bernard Parish suffered near complete inundation. Its loss of population during the decade after Katrina (from 2000 to 2010) was proportionally larger than that of any other parish in the study area. Between 2000 and 2010, the population of St. Bernard dropped by 31,000; between those years, Plaquemines lost 3700 residents. Over two decades later, the demographic profile of the study area has changed significantly; in Orleans Parish, the percentage of Black residents declined from 67% in 2000 to approximately 54% in 2025. Similarly, in that same time frame, the percentage of white residents increased from approximately 28% to roughly 32%. Finally, the percentage of Hispanic residents tripled from approximately 3% in 2000 to roughly 9 percent in 2025. As of 2019, approximately 100,000 fewer people were living in New Orleans than existed at the time of the hurricane (a number equal to that of Black residents who did not return), illustrating how Katrina's demographic legacy is intertwined with both racialized geographic patterns of displacement and nonreturn. This study seeks to spatialize using its trajectory and clustering analyses.

Hurricane Katrina landed as a category three hurricane on 29th August 2005. Catastrophic failure of the levees resulted in around 80% of New Orleans being flooded. Estimates suggest that the storm caused approximately 1833 deaths and $125 billion worth of damage (Kates et al. 2006; Olshansky et al. 2008). The five parishes had very varying degrees of impact: Orleans and St. Bernard Parishes were largely inundated, and both lost large numbers of homes; Jefferson Parish was badly damaged but remained operational compared to the other four; Plaquemines Parish suffered significant coastal surge damage; and St. Charles Parish suffered less extensive urban flooding (Kamel 2012; Fraser et al. 2022). It is the vastly different levels of damage, along with the differing capacity for governance and socio-economic characteristics of each parish, that make

these five parishes such an ideal case study for identifying and comparing different recovery processes.

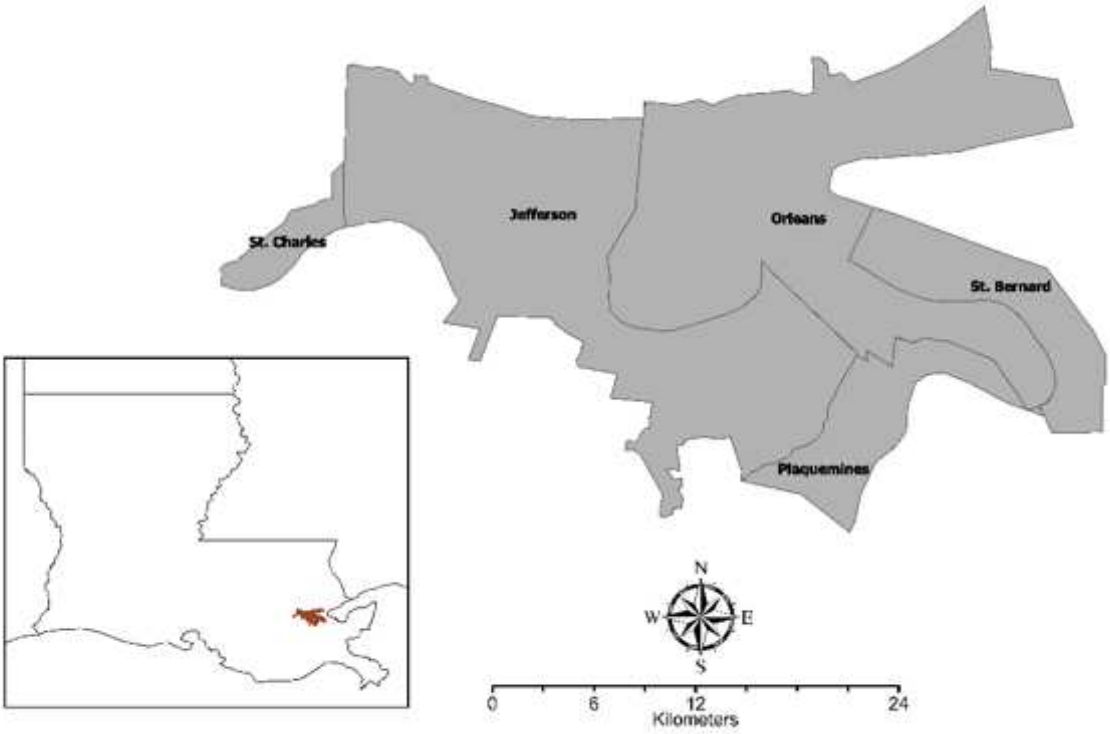


Fig. 1 The five-parish Greater New Orleans metropolitan region

3. Data and Methods

3.1. Satellite Imagery Acquisition

Seven epochs of images captured on cloud screens were obtained to document the 21-year time frame, from the baseline before Katrina, immediately after Katrina, and through the full recovery of the wetlands (Table 1). The surface reflectance data products for Landsat 5 TM (2004, 2005, 2009), Landsat 8 OLI (2013, 2017) were collected from the U.S. Geological Survey's EarthExplorer Archive at 30m resolution. In addition, Level-2A images from the Sentinel-2 Multi-Spectral Instrument (MSI) were downloaded from Google Earth Engine (GEE) for two years (i.e., 2021, 2025). All the images were chosen based upon having less than ten percent cloud cover

during the dry season (i.e., June – September) to minimize variation due to phenology. Satellite imagery combined with machine learning offers a scalable, publicly accessible means of quantifying hurricane impacts across entire urban regions (Composto et al. 2025).

Where it was impossible to find an individual image that had less than five percent cloud cover, cloud-free composites were created by using GEE Median Compositing with a 45-day window (Gorelick et al. 2017). Satellite-derived observations allow hurricane impacts to be assessed at large spatial extents while retaining structure-level resolution, reducing the uncertainty introduced by statistical extrapolation from aggregated data (Miller et al. 2021).

Table 1 multi-temporal satellite imagery dataset.

Sensor	Years	Resolution	Source
Landsat 5 TM	2004, 2005, 2009	30 m	USGS Earth Explorer
Landsat 8 OLI	2013, 2017	30 m	USGS Earth Explorer
Sentinel-2 MSI	2021, 2025	10–20 m	GEE
SRTM/LIDAR DEM	Static	30 m	USGS / NOAA
OSM Roads & Buildings	2024 extract	Vector	Geofabrik (geofabrik.de)
Building Footprints	2020	Vector	Microsoft / NOAA

3.2. Resolution Harmonization

Bands from the Sentinel-2 MSI satellite with 10m and 20m pixel sizes have been resampled to 30m using bilinear interpolation via GEE's reproject () function for compatibility with Landsat spatial grids. The cross-sensor harmonization followed previously established methods (Chastain et al. 2019) which ensured that inter-annual variability in land cover was not caused by the difference in spatial scales between Landsat and Sentinel-2, or by differences in spatial scale in ancillary data (DEM, road networks) on which neighborhood clusters are based.

3.3. Land Cover Classification Scheme and Training Sample Design

Four land cover classes were determined with respect to the dominant surface characteristics of a coastal delta (Table 2). The four classes were developed using classification

methods previously used in studies of wetlands affected by urbanization in Louisiana (Dronova et al. 2012; Couvillion et al. 2017). For each year, 450 reference points were created using the Select Feature option in ArcGIS Pro. Allocation of sample size for each class was based upon both the relative frequency of occurrence and spectral heterogeneity of the respective classes (Table 3). As there is considerable intra-class variability associated with this class due to various rooftop surfaces and materials, Built-Up received the most allocations (200) among all classes. Each of the remaining two classes, Water and Forested Wetland, received an equal number of allocations (100) since they have similar amounts of space and are spectrally complex. Because of minimal spectral differences occurring among members of this class, Vegetation had the least number of allocations (50).

Table 2 Four-class land cover scheme.

Class	Name	Description
1	Water	Open water: Mississippi River, Lake Pontchartrain, tidal channels, canals, and inundated surfaces.
2	Built-up	Impervious surfaces: buildings, rooftops, roads, parking lots, and paved infrastructure.
3	Vegetation	Herbaceous and low woody cover: lawns, scrubs, emergent marsh, and agricultural fields.
4	Forested Wetland	Woody wetland: cypress-tupelo swamps, bottomland hardwoods, and mangrove-dominated areas.

Table 3 Training sample allocation by land cover class.

Class	n	% Total	Rationale
Water	100	22.2	Variable spectral response across water clarity and depth
Built-up	200	44.4	High intra-class variability; diverse roof and pavement types
Vegetation	50	11.1	Spectrally homogeneous; smaller spatial extent
Forested Wetland	100	22.2	Confusion risk with Vegetation; critical for wetland change detection
Total	450	100	

3.4. Spectral Feature Engineering

Each of the epoch's images consisted of 20 input features: 6 raw Spectral Bands (Blue, Green, Red, NIR, SWIR1 & SWIR2) and 14 Derived Spectral Indices (Table 4). The choice of indices was based on their ability to represent the Vegetation Vigor (NDVI, EVI, SAVI, MSAVI, VARI & GNDVI); Water Presence and Soil Moisture (NDWI, MNDWI & NDMI); Urban Impervious Surfaces (NDBI, BSI, UI); Fire Severity/Burn Recovery (NBR); and Bare Mineral Soil (NDSI) - an Engineering Feature approach that is comparable to High Accuracy Multi-Class Classification in Coastal Environments with High Spectral Complexity (Breiman 2001; Dronova et al. 2012; Zhao and Qin 2019). All Indexes were calculated using a Python script combined into a twenty-one-band composite for each epoch.

Table 4 Spectral feature stack: 15 derived indices + 6 raw spectral bands = 20 features total per epoch.

Index	Full Name	Formula	Thematic Purpose
NDVI	Normalized Difference Vegetation Index	$\frac{(NIR-Red)}{(NIR+Red)}$	Vegetation vigor
EVI	Enhanced Vegetation Index	$\frac{(2.5\ x\ (NIR-RED)}{(NIR+\ 6Red-7.5Blue+1)}$	Canopy structure & LAI
SAVI	Soil-Adjusted Vegetation Index	$\frac{(NIR-Red)}{((\mathrm{NIR+Red+0.5})\times 1.5))}$	Sparse-soil vegetation
MSAVI	Modified SAVI	$\frac{(2NIR+1-\sqrt{(2NIR+1)^2-8(NIR-Red)})}{2}$	Low-density vegetation
VARI	Visible Atmospherically Resistant Index	$\frac{(Green-Red)}{(Green+Red-Blue)}$	Visible-range vegetation
GNDVI	Green NDVI	$\frac{(\mathrm{NIR-Green})}{(\mathrm{NIR+Green})}$	Chlorophyll concentration
NDWI	Normalized Difference Water Index	$\frac{(\mathrm{Green-NIR})}{(\mathrm{Green+NIR})}$	Open water detection
MNDWI	Modified NDWI	$\frac{(Green-SWIR1)}{(Green+SWIR1)}$	Turbid / shallow water
NDMI	Normalized Difference Moisture Index	$\frac{(\mathrm{NIR-SWIR1})}{(\mathrm{NIR+SWIR1})}$	Vegetation moisture
NDBI	Normalized Difference Built-up Index	$\frac{(SWIR1-NIR)}{(SWIR1+NIR)}$	Urban surfaces
BSI	Bare Soil Index	$\frac{(\mathrm{SWIR1+Red})-(\mathrm{NIR+Blue})}{(\mathrm{SWIR1+Red})+(\mathrm{NIR+Blue})}$	Bare soil / exposed land
UI	Urban Index	$\frac{(\mathrm{SWIR2-NIR})}{(\mathrm{SWIR2+NIR})}$	Urban density proxy

NBR	Normalized Burn Ratio	$\frac{(\text{NIR}-\text{SWIR2})}{(\text{NIR}+\text{SWIR2})}$	Burn severity / vegetation recovery
NDSI	Normalized Difference Snow Index	$\frac{(\text{Green}-\text{SWIR1})}{(\text{Green}+\text{SWIR1})}$	Bare mineral / soil
BLUE	Blue Band	$Raw\ \rho\ (B2)$	Atmospheric scattering baseline
GREEN	Green Band	$Raw\ \rho\ (B3)$	Vegetation / water spectral peak
RED	Red Band	$Raw\ \rho\ (B4)$	Chlorophyll absorption
NIR	Near-Infrared	$Raw\ \rho\ (B8/B5)$	Vegetation canopy contrast
SWIR1	Short-Wave IR 1	$Raw\ \rho\ (B11/B6)$	Soil moisture / urban
SWIR2	Short-Wave IR 2	$Raw\ \rho\ (B12/B7)$	Geology / fire severity

3.5. Machine Learning Classification

A Random Forest (Breiman 2001), often called a base or benchmark model, was used as the benchmark classifier. It constructs a set of decision trees by randomly sampling data subsets and selecting a subset of features at each node. This approach helps prevent overfitting, particularly in high-dimensional spectral data, which is why it is the most studied algorithm in remote sensing land cover classification (Belgiu and Drăguţ 2016). The RF classifier was built with 200 trees and limited the number of features used for splitting to no more than $\sqrt{21} \approx 5$. Support Vector Machines (SVM) with a radial basis function kernel and K-Nearest Neighbors (k=5) were employed as comparison models. Subsequently, Extreme Gradient Boosting (XGBoost; Chen and Guestrin, 2016) was selected as the main model because it demonstrated superior accuracy over Random Forests when classifying spectrally diverse areas (Maxwell et al. 2018). The XGBoost was configured with several parameters, including a learning rate (η = 0.05), maximum tree depth (max_depth=6), sampling ratio (subsample=0.85), column sampling ratio (colsample_bytree =

0.85), number of boosting rounds (boost_rounds=300), and early stopping with a patience of 20 to monitor performance on 20% of the training data, reserved for cross-validation purposes. Each model is fitted separately to each of the seven-time steps.

3.6. Accuracy Assessment: Spatial Split Cross-Validation

Classification accuracy was tested with respect to an independently stratified testing sample (200 observations; 30 by classification group) as measured by Overall Accuracy (OA), Producer's Accuracy (PA), User's Accuracy (UA), and Kappa coefficient (κ). A spatial split cross-validation approach was applied to reduce the effects of spatial autocorrelation that have been documented (Roberts et al. 2017) to be one of several sources of artificially increased accuracy in geospatial machine learning. Each spatial block was created based on a 5km x 5km grid cell size. In each iteration of the k-fold cross-validation method, all observations from a single test block served as the testing sample while all other blocks served as the training samples, thereby preventing any spatially adjacent training/testing sample pairings (Valavi et al. 2018). The confusion matrices were developed for all 28 outputs (7 epoch iterations x 4 classifier types).

3.7. SHAP Feature Importance Analysis

Shapley additive explanations (SHAP) for each epoch's fitted XGBoost model were computed for every epoch (using the (Lundberg and Lee 2017) methodology), as this offers a decomposition of each prediction that can be attributed to specific input data elements (i.e., per-feature contributions). The mean absolute SHAP values (mean |SHAP|) of all training samples per epoch produced a 20 x 7 feature-importance matrix. Unlike XGBoost's gain-based feature importance, SHAP is grounded in cooperative game theory, making it both unbiased toward higher cardinality features (Lundberg et al. 2020) and statistically consistent with its application. Stacked bar plots of per-class SHAP values were also generated for the 2004 baseline and 2025

contemporary epochs to identify which spectral features contributed to discriminating against each land-cover class. The calculations used to create these SHAP values were performed via the SHAP Python library.

3.8. Urban Intensity Index Change Analysis

The authors calculated the Urban Intensity Index (UII) for the images of 2005 and 2025 at the pixel level to characterize sub-category variations in urban surface density based on the classifications of land use/land cover that are binary. The authors used the same logic behind the spectral contrasts presented in (Weng et al. 2004) and (Xu 2008), which is to combine two indices sensitive to built-up surfaces and suppress vegetation by creating an index utilizing the opposite spectral responses of built-up surfaces and vegetation. The authors created this index as follows for both years:

$$UII = NDBI + BSI - NDVI$$

In the above equation, NDBI (Normalized Difference Built-up Index) and BSI (Bare Soil Index) have positive values when they represent impervious and/or bare surfaces, while NDVI (Normalized Difference Vegetation Index) has negative weights, suppressing vegetated pixels and amplifying the contrast between urban and non-urban surfaces. The authors then utilized the 20-band spectral feature stack to calculate the NDBI (band position 10), BSI (band position 11), and NDVI (band position 1). Each of these indices was calculated in detail according to section 3.4. All calculations were completed in EPSG:32615 (UTM Zone 15 North) to provide consistent metrics across the entire study area.

Analysis was restricted to pixels intersecting a single building footprint mask derived from the Microsoft Building Footprints dataset. The same footprint layer was applied to both the 2005 and 2025 epochs, so ΔUII was computed over an identical set of pixels in both years. The footprints

were reprojected to EPSG:32615, clipped to the raster extent, and buffered by 15 m to allow for positional error at building edges. A spatial index was used to speed up the identification of footprints intersecting each raster window, and because the study area exceeded available memory, the rasters were processed in 512 × 512-pixel tiles. Footprints were rasterised with the all-touched option enabled, and pixels outside the buffered mask were assigned to NoData. Pixel-wise calculation of UII change was done using the following equation:

$$\Delta UII = UII_{2025} - UII_{2005}$$

where positive values indicated an increase in urban surface intensity and negative values indicated a decrease in urban surface intensity. Distributions of parish-level ΔUII were compared to $\mu = 0$ to identify if there were statistical increases or decreases in intensity per parish through one-sample t-tests.

3.9. Temporal Trajectory Analysis

Besides identifying category 2 -- "stable built-up" (built-up at all three time epochs) and category 3 -- "new built-up / regeneration" (non-built-up in 2004/2005 that became built-up in a subsequent epoch and remained built-up), the remaining categories captured the full range of land cover dynamics across the study area. Category 4 -- "built-up loss" identified pixels that were built-up in 2004 but had not recovered built-up status by the final epoch, representing permanent abandonment or conversion. Category 6 -- "fluctuating built-up" captured pixels with multiple alternating transitions between built-up and non-built-up states, reflecting marginal land instability or spectral ambiguity at the urban-wetland interface. Categories 1 and 7 -- "water" and "other dynamic non-built" encompass persistent and transitional non-urban surfaces, including open water bodies, wetlands, and ecologically dynamic coastal margins. Category 5 -- "decline then recovery" revealed a unique post-disaster signature of urban regeneration. Category 5 includes

pixels that were built-up in 2004 but were destroyed after Hurricane Katrina, then rebuilt by 2013 or later.

Table 5 Seven-category pixel-level temporal trajectory classification scheme.

Code	Category	Definition
1	Water	Non-built up in all seven epochs; persistent natural or semi-natural surface with no evidence of urban development.
2	Stable Built-up	Built-up in all seven epochs; enduring urban fabric through the disturbance period.
3	New Built-up / Regeneration	Transitions from non-built-up (≤2005) to built-up in subsequent epochs and remains built-up; greenfield or delayed regeneration.
4	Built-up Loss	Built-up in 2004/2005, transitions to non-built-up without subsequent recovery; permanent abandonment or land conversion.
5	Decline then Recovery	Built-up 2004, non-built-up 2005/2009, returns to built-up 2013 or later; direct spatial footprint of post-disaster urban regeneration.
6	Fluctuating Built-up	Multiple alternating transitions; marginal land, urban fringe instability, or spectral classification ambiguity.
7	Other Dynamic Non-Built	Transitions within non-built-up classes only; wetland succession, tidal flooding, and storm-driven ecological change.

3.10. Spatial Autocorrelation Analysis: Global Moran's I and LISA

To determine whether spatial relationships existed in the class-specific trajectory proportions, the Global Moran's I statistics for these proportions were calculated. A local measure of spatial association called LISA was also utilized (Anselin 1995); both were calculated at the census tract level. To do so, a ratio of the number of pixels per census tract (representing each of our seven trajectory classes) was calculated. These ratios were computed for all seven classes from the XGBoost-based trajectory rasters. The resulting ratios for each census tract served as spatially referenced attributes. Finally, a queen-contiguity spatial weights matrix was created from the census tract polygons, standardized by rows, and then Global Moran's I was calculated. Global Moran's I was computed as:

$$I = (n/(S_0)) * ([\Sigma_i \Sigma_j w_{ij}(x_i - \bar{x})(x_j - \bar{x})])/(\Sigma_i((x_i - \bar{x})^2)$$

where n = number of census tracts; S_0 = Sum of all spatial weights; w_{ij} = Spatial weight for tracts i and j; x_i = Proportion of each tract's trajectory class. Pseudo p-values from 999 permutations were used to test statistical significance. The LISA method identifies four local association types in each tract: HH (Hot Spot) = High-High, LL (Cold Spot) = Low-Low, HL (Spatial Outlier - High surrounded by Low) = High-Low, LH (Spatial Outlier - Low surrounded by High) = Low-High.

3.11. Neighborhood Typology Clustering

A multivariate feature matrix was developed for census tracts based on geographically aggregated data across three categories of input data, with the New Orleans census tract geographic boundaries. Census tract shapefiles were used as the primary spatial units of analysis in this research, but no socio-demographic data were included in the feature space for the k-means clustering. Average and minimum tract elevations were extracted from a 30m DEM and treated as direct proxies for flood risk. Tract average elevation represents the typical elevation of each tract, whereas minimum elevation is the lowest elevation within the tract boundary that determines the worst-case scenario for flooding (Qiang and Lam 2016). The proportion of pixels associated with each of the seven temporal trajectory classifications -- Water, Stable Built-up, New Built-up/Regeneration, Built-up Loss, Decline and then Recovered, Fluctuating Built-up, and Other Dynamic Non-Built was calculated on a census tract basis from the XGBoost-generated pixel-level trajectory raster. This embedded the twenty-year history of post-Katrina land use changes in the feature space and made the composition of trajectories the driving force behind neighborhood differences. In addition to these two variables, two new infrastructure accessibility metrics were also created from OpenStreetMap (OSM) road and building layer data.

These two new metric variables were the mean Euclidean distance between each census tract centroid and its closest OSM road segment (used as a proxy for connectivity), and the mean

Euclidean distance between the edge of each tract and the center of the closest OSM building footprint (a measure of compactness/spatial density in terms of built environment features). Both OSM metrics were created by applying GeoPandas spatial joins and distances calculations to the clipped versions of OSM layers.

Prior to clustering, all variables were standardized using Z-Score Standardization, so that scale would have no effect on the calculation of Euclidean distance metrics. The K-Means Clustering algorithm was run on the standardized feature matrix. Two methods were used to determine an optimal number of clusters: (1) the Elbow method (using the Within Cluster Sum of Squares or WCSS) and (2) Silhouette Scores (Rousseeuw 1987). K=4 was selected at the elbow of the WCSS curve; although K=2 had the highest Silhouette score, K=4 gave interpretable and spatially consistent neighborhood types where there was a clear elbow in the WCSS plot, resulting in four clearly identifiable and spatially consistent neighborhood types.

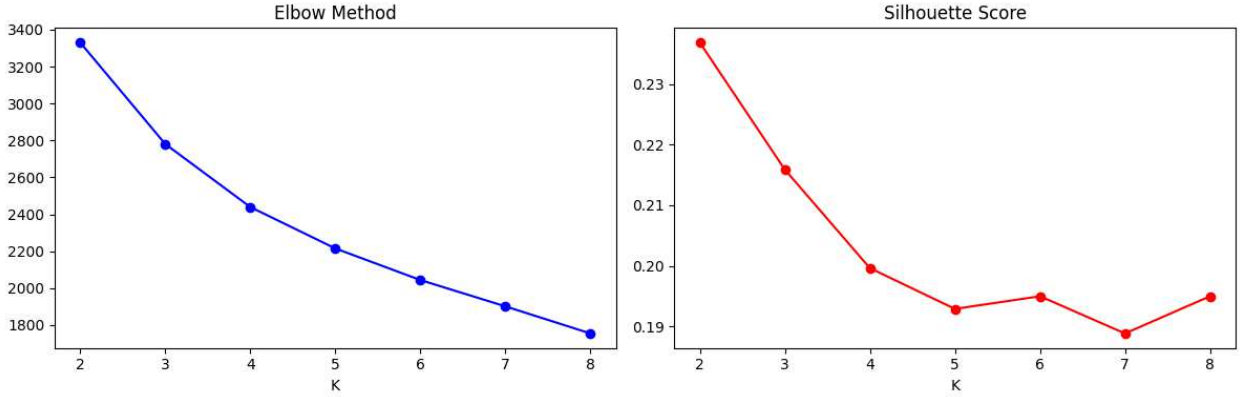


Fig. 2 Cluster validity metrics for neighborhood typology K selection

4. Results

4.1. Classification Accuracy

The accuracy level of the 4 classification methods is given in Table 6. However, XGBoost and RF have similar performance on most epochs. However, XGBoost equals RF in 2005 (97.8%) and exceeds it in 2021 (93.4% vs 92.2%). XGBoost OA has been between 93.4% (2021) and 99.3%

(2004); its Kappa coefficients range from 0.902-0.990. The lowest accuracy was observed in the 2021 epoch, affecting all classifier models. This may be due to land-cover changes at the wetland margin resulting from active post-hurricane vegetative recovery and tidal readjustment. All four classifiers were competitive; KNN had the lowest accuracy in 2005 (96.7%), likely due to spectral ambiguity.

Table 6 Spatial split cross-validation accuracy for all four classifiers across seven epochs. OA = Overall Accuracy; κ = Kappa coefficient

Classifier	2004	2005	2009	2013	2017	2021	2025
XGBoost (OA %)	99.3	97.8	98.6	98.5	97.8	93.4	97.0
XGBoost (κ)	0.990	0.968	0.979	0.977	0.967	0.902	0.955
RF (OA %)	99.7	97.8	98.6	98.5	97.4	92.2	96.7
RF (κ)	0.996	0.968	0.979	0.979	0.961	0.884	0.951
SVM (OA %)	99.7	97.6	98.8	98.8	98.6	94.4	97.7
SVM (κ)	0.996	0.966	0.982	0.983	0.980	0.917	0.965
KNN (OA %)	99.9	96.7	97.8	98.4	97.8	93.2	97.1
KNN (κ)	0.998	0.952	0.967	0.976	0.967	0.899	0.957

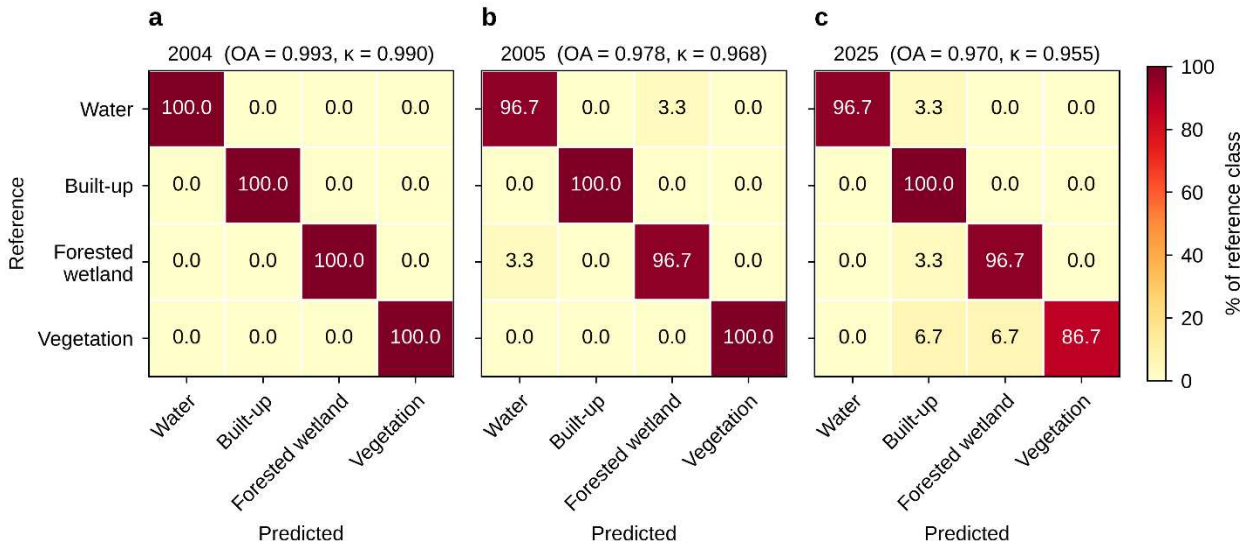


Fig. 3 XGBoost confusion matrices for selected epochs

4.2. SHAP Feature Importance Analysis

SHAP values are used to decompose a model into individual variables and to determine how much each variable contributed to the output. In this case, the SHAP values reveal both a physical and interpretive relationship among the classification epochs. As we can see in Figures 4a and 4b, there were large, systematic differences in the contributions made to the classifications by the 20 features during the seven different epochs. As seen in Figure 4a, the first epoch in the time series was the undisturbed pre-Katrina baseline (2004). At this time, the EVI band had the greatest contribution toward classification (Mean |SHAP| = .63), followed closely by the NIR (0.57), BLUE (.52), and SWIR1 (0.46). These results indicate that EVI and NIR have a high degree of spectral significance when distinguishing between forested wetlands and/or vegetation from other land use/cover types, such as built-up or water, in an unaltered coastal deltaic environment.

A per-class SHAP analysis confirmed that the importance of EVI was split between the discrimination of forested wetlands/vegetation and discrimination of built-up/water; whereas SWIR1 was important only in separating water from built-up pixels. Of interest, NDBI, which is often referred to as the index of choice in many urban studies (Weng et al. 2004; Fussell et al. 2014), was the least significant contributor to the classifications in every epoch (Mean |SHAP| < 0.004 in 2004, Max = 0.092 across all epochs). The 2005 post-inundation epoch resulted in the most unique SHAP profile in the dataset. At this time, the BLUE band represented the highest single-band/single-epoch value recorded at Mean |SHAP| = 0.88.

Physically speaking, these results can be attributed to the spectral signature associated with standing bodies of floodwater. Standing bodies of floodwaters result in enhanced reflectance in the blue portion of the spectrum due to rough surface and reduced near infrared reflectance due to suppression of plant canopy; thus, providing a diagnostic signal that could easily be distinguished by the XGBoost classifier. Consistent with the fact that numerous parcels of developed lands

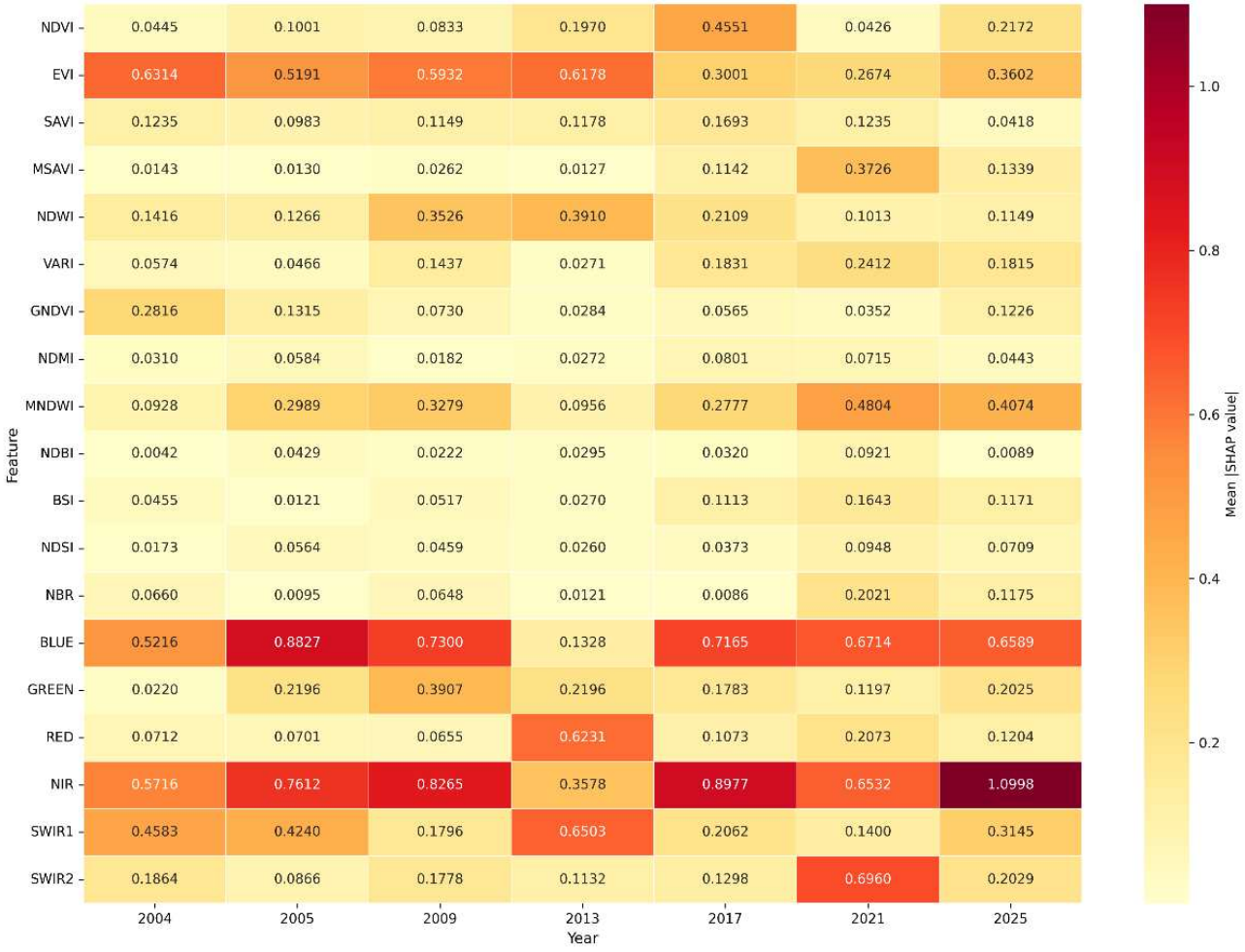
362 throughout Orleans and St. Bernard parishes were inundated with water bodies of standing
363 waters/turbid flooded surfaces immediately following Hurricane Katrina, NIR remained as the
364 second most important band (0.76); while MNDWI and GREEN demonstrated increases in
365 importance over those observed in 2004 consistent with widespread presence of shallow bodies of
366 standing waters/turbid flooded surfaces.

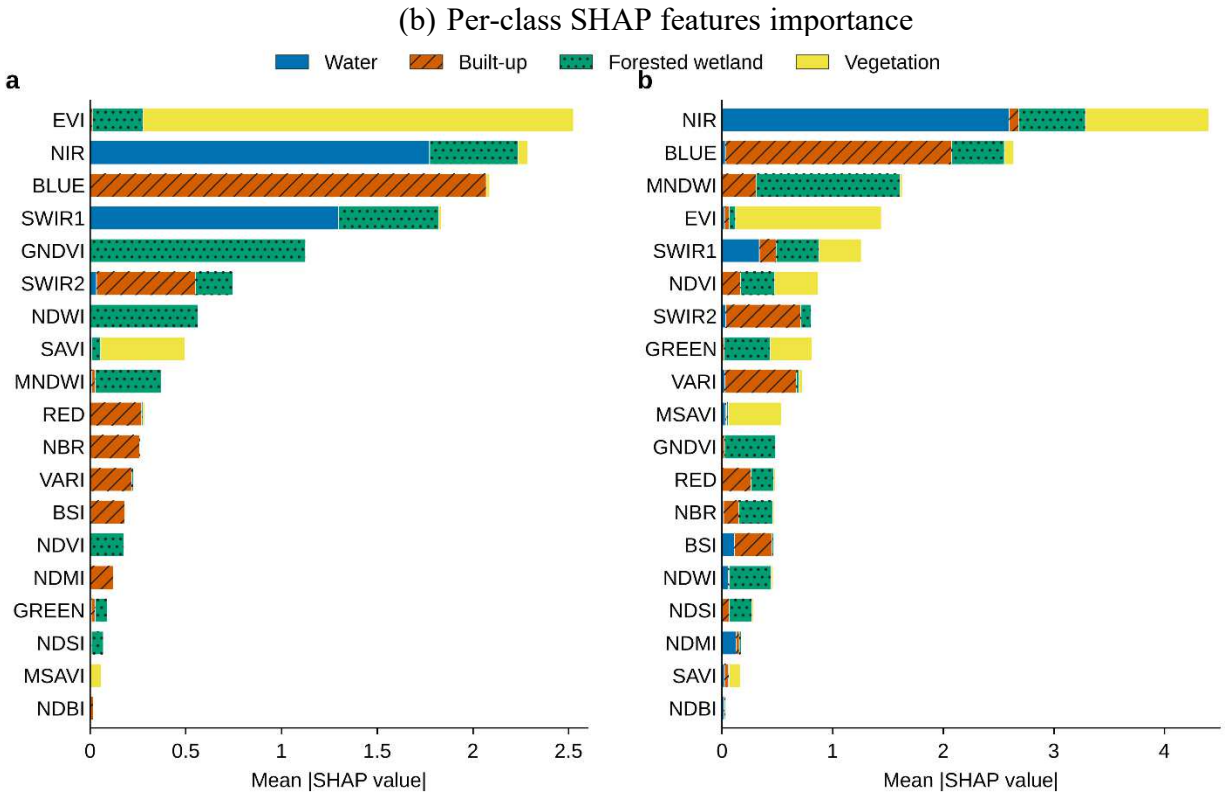
367 During the early recovery periods (2009), BLUE (0.73) and NIR (0.83) continued to
368 demonstrate dominance. However, MNDWI was elevated (0.33), consistent with prolonged
369 periods of saturated soils and partial waterlogging of many areas being drained after Hurricane
370 Katrina. Through the latter part of the recovery period (2013), RED (0.62) and SWIR1 (0.65)
371 became increasingly important, and it is reasonable to infer that these bands represent the spectral
372 signatures of exposed building materials and disturbed soils on many of the active
373 construction/rebuilding sites. By 2017, NIR reached its highest values during the recovery period
374 (0.90), and BLUE continued to show high levels of importance (0.72). It is interesting to note that
375 MNDWI showed its highest level of importance across all epochs at 2021 (0.48), which correlates
376 temporally with the maximum amount of post-hurricane Katrina wetland adjustments and tidal
377 recoveries occurring along the coastal margins of Plaquemines and St. Bernard parishes.

378 In 2025, NIR demonstrated its highest level of importance ever recorded across the entire
379 21-year analytical window through a Mean |SHAP| value of 1.10 and became the most important
380 feature, surpassing BLUE (0.66) by a wide margin. Additionally, per-class SHAP analysis for
381 2025 indicates that NIR's strong dominance is distributed across all four classes; however, it is
382 strongest for Water and Vegetation discrimination. This represents spectral maturity to the post-
383 Hurricane Katrina landscape, where two decades of wetland ecological succession and suburban
384 vegetation growth resulted in an increase in near-infrared reflectance contrast between classes.

MNDWI (0.41) continued to be significantly elevated in 2025 as shown in Figure 4c, consistent with wetland moisture signals persisting along the southern and eastern margins of the study area.

(a) Features importance heatmap





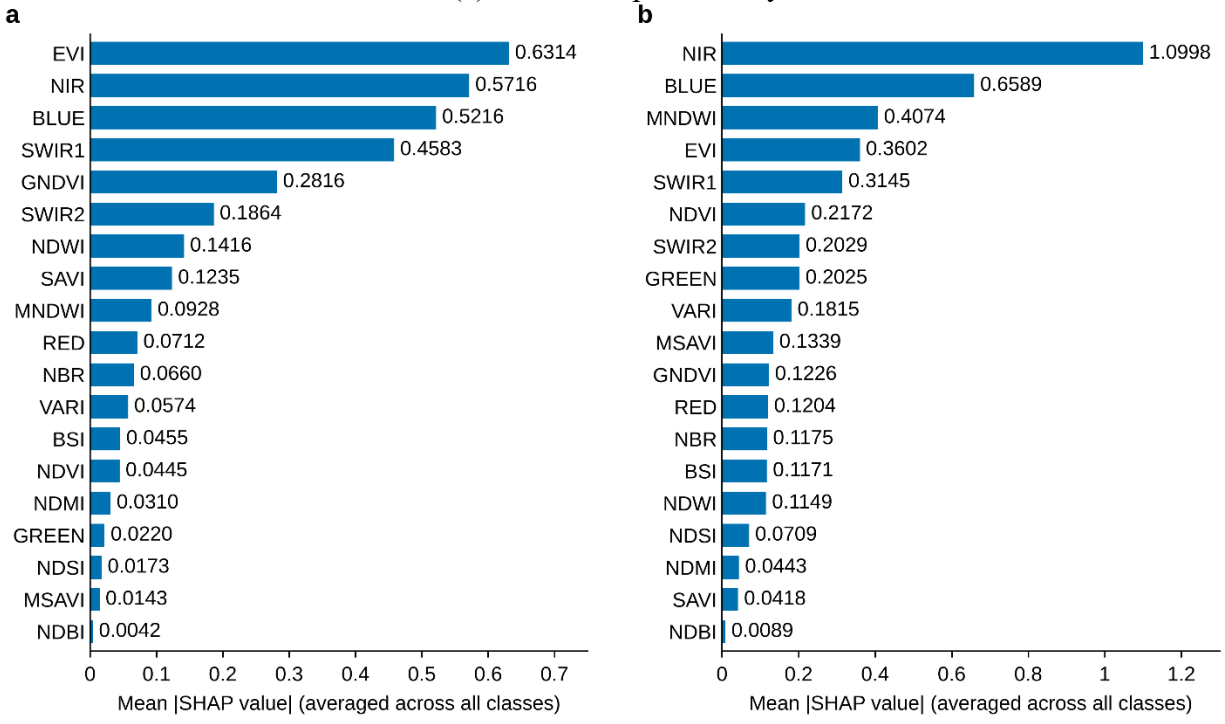


Fig. 4a XGBoost SHAP features importance heatmap across all seven epochs. Darker cells indicate stronger influence on classification decisions. **b** Per-class SHAP feature importance for 2004 (pre-Katrina baseline) and 2025

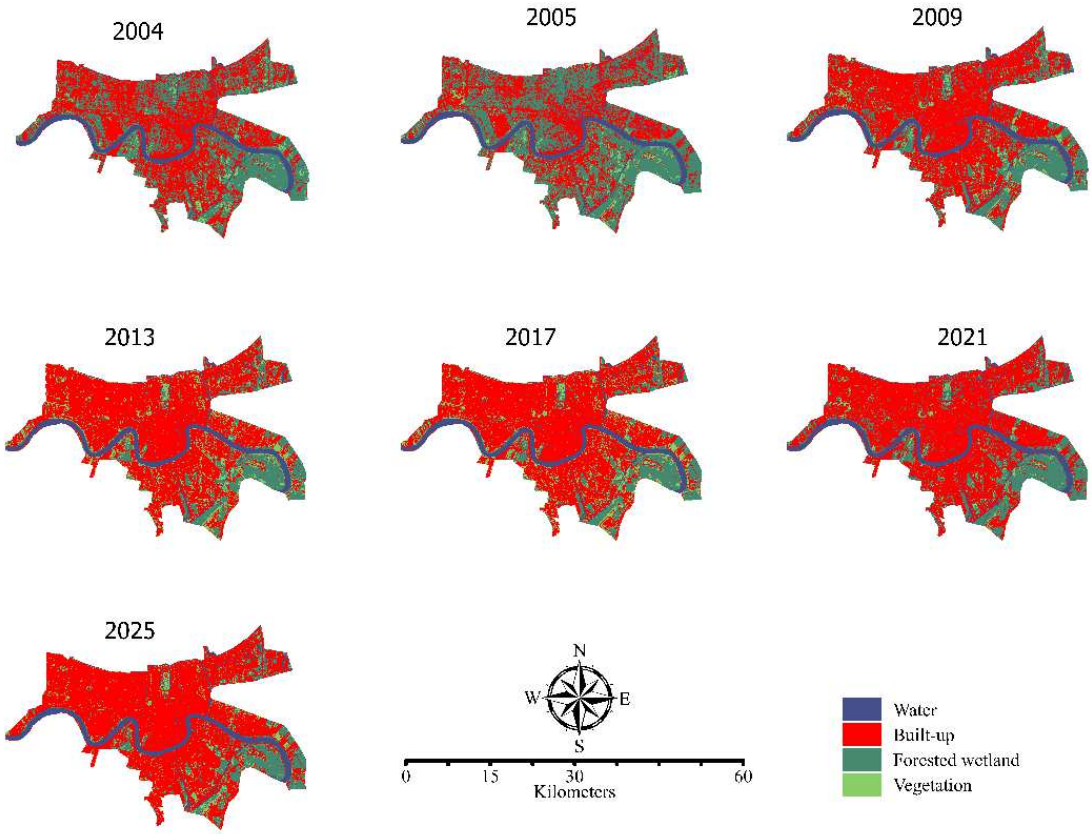
(contemporary epoch), illustrating class-level spectral drivers of XGBoost classification. **c** Ranked XGBoost feature importance by mean |SHAP| for 2004 and 2025

4.3. Multi-Temporal Land Cover Change

The XGBoost classification output shows an extremely nonlinear development of land cover transition over time in response to Hurricane Katrina and its aftermath (Figure 5a), similar to the overall trajectory of the hurricane's damage and recovery. Developed areas fell significantly from 2004 to 2005 due to severe flooding that turned previously developed areas into open waters throughout Orleans and St. Bernard Parishes, which is also consistent with reports of massive flooding of residential and commercial areas during those years (Homeland Security, Federal Emergency Management Administration (FEMA) 2006).

The built-up area began to recover slowly by 2009, indicating the low levels of early-stage population growth reported by (Fussell et al. 2014). Continued significant growth in the amount of built-up area occurred through 2009 – 2017 at a slightly increasing rate towards 2025, when long-term funding for CDBG-DR disbursement and Road Home grants began to be implemented - this timing matches the housing recovery timeline analyzed by (Kondo 2017b). Forested wetland declined continuously in most of the seven time periods - a regional trend caused by deltaic subsidence and saltwater intrusion that existed prior to the storm and was intensified but not created by the storm (Chuang et al. 2019). The water class increased between 2004 and 2005 (after the storm flooding) to 2013, then declined in the years following recovery from the 2005 flood event (Figure 5b).

(a) XGBoost Land cover classification maps



(b) Land cover area changes (km^2)

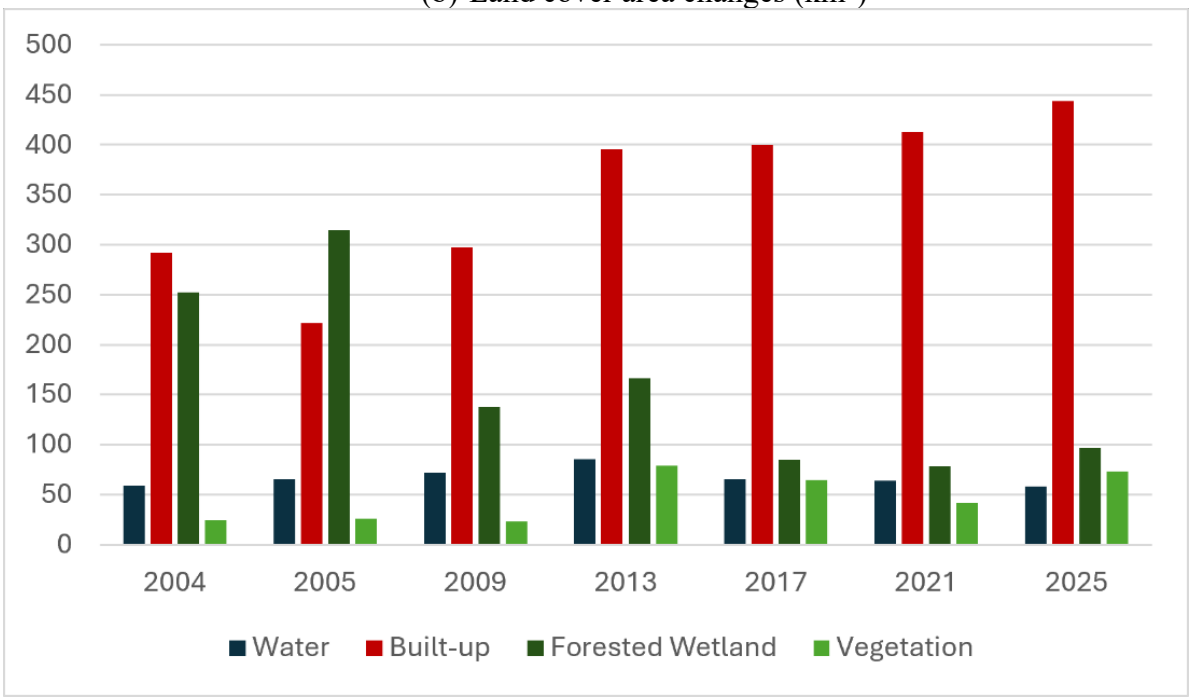


Fig. 5a XGBoost land cover classification maps, Greater New Orleans five-parish study area, 2004–2025. **b** Land cover class area changes (km^2), Greater New Orleans five-parish study area, 2004–2025 (XGBoost classification)

4.4. Urban Intensity Index Change (2005–2025)

Changes in the Urban Intensity Index across the parishes are illustrated in Figure 6. The average increase in UII for the Metropolitan Area was 0.18 (σ = 0.21); t-test results show a difference from 0 with a t-value of 12.4 (p-value < .01). This indicates there was a statistically significant amount of net urbanization occurring within the post-Katrina period across the metropolitan area. Additionally, parish-level t-tests showed that each of the three parishes that had the greatest levels of urban intensification was positively affected as well. These included Jefferson (+0.24; p-value < .01), St. Charles (+0.21; p-value < .01), and Orleans (+0.11; p-value = .03).

Although the other two parishes suffered damage during Katrina and experienced some urban growth, neither St. Bernard (+0.09; p-value = .07) nor Plaquemines (+0.07; p-value = .12) reached the 5% level of confidence required for statistical significance indicating that any urban

densification that occurred in those two parishes as a result of the storm was limited. Strongly positive values for ΔUII (ΔUII ≥ +0.30) are evident throughout the neighborhoods of Lakeview and Mid City (Orleans Parish), the eastside suburban expansion zones of Jefferson Parish, and commercial corridors along the US-90 corridor in St. Charles Parish, all areas that have relatively high elevation and received both public and private funding after the storm. Negative values for ΔUII (ΔUII ≤ -0.20) are observed in the lower Ninth Ward and New Orleans east, where few residents returned to their homes resulting in a decrease in residential parcels being occupied, and an increase in vacant lot development and thus a loss of urban density (Kamel 2012); (Lewis et al. 2017).

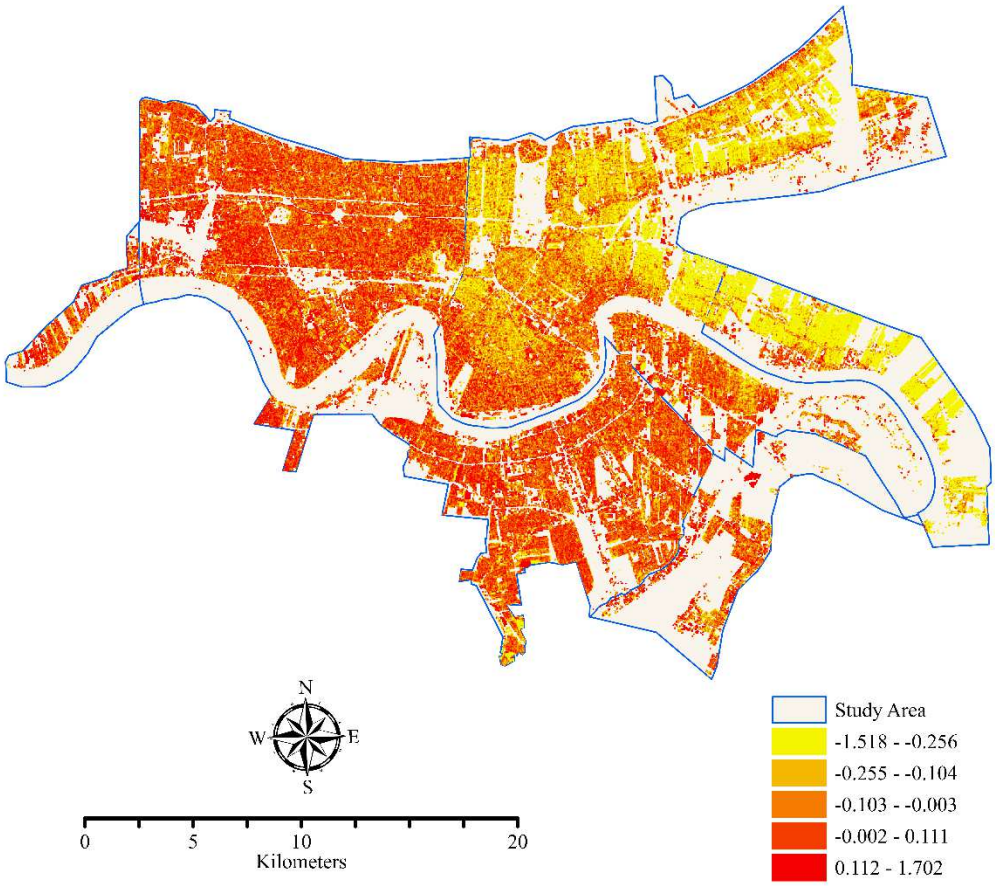


Fig. 6 Urban Intensity Index Change (ΔUII), 2005–2025. Positive = densification; negative = decline. Building footprint masks applied

4.5. Temporal Trajectory Analysis

The pixel-level trajectory classification applied to all seven XGBoost maps reveals the full spatiotemporal structure of urban transformation across the study area (Table 7; Figure 7).

Table 7: Temporal trajectory category area statistics derived from seven-epoch XGBoost classification stack (30 m pixel resolution)

Code	Category	Pixel Count	Area (km^2)
1	Water	76,429	68.79
2	Stable Built-up	187,062	168.36
3	New Built-up / Regeneration	101,836	91.65
4	Built-up Loss	2,177	1.96
5	Decline then Recovery	108,755	97.88
6	Fluctuating Built-up	49,762	44.79
7	Other Dynamic Non-Built	170,556	153.50
	Total	696,577	626.92

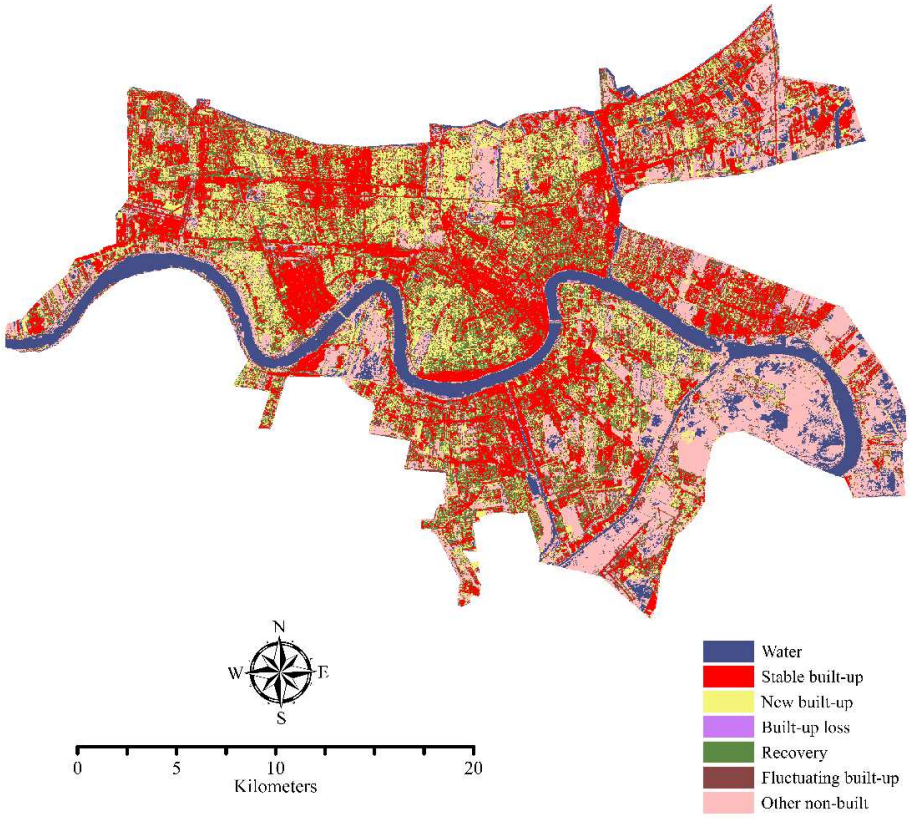


Fig. 7 Spatial distribution of the seven temporal trajectory categories derived from the seven-epoch XGBoost classification stack

Class 2 represents the stable built-up land (168.36 km^2) as the greatest individual classification of land use. Land classified as Class 2 exists primarily on the higher levees of the Mississippi River located within Orleans and Jefferson parishes, where flooding caused by Katrina was significantly less than other parts of the study region. The positive relationship between elevation and development also parallels the work of Qiang and Lam (2016), demonstrating that after Katrina, there existed an increased likelihood of urban growth in Louisiana as a function of elevation. Similarly, Class 1, representing the Water category, exists primarily at the borders of the study region, including the wetlands and open water bodies of Plaquemines and St. Bernard parishes.

Transitioning into new build or redevelopment classifications, Class 3 represents land uses that were previously non-buildable land but have transitioned into built-up land categories. A substantial number of these transitions took place between the years 2009 and 2013, coinciding with peak funding for CDBG-DR (Community Development Block Grants – Disaster Relief) and Road Home (U.S. Department of Housing and Urban Development 2007). A secondary peak in transition activity occurred during the years 2017 through 2021, which represents a period of delayed recovery occurring in the second post-Katrina decade (Kondo 2017a).

The analytically most important category is Class 5 (decline then recovery) because it captures the specific spatial location of the post-Katrina urban regeneration process. The primary locations represented by Class 5 include New Orleans East, Gentilly, Lakeview, Chalmette (St. Bernard Parish), and parts of Harvey and Marrero (Jefferson Parish) - neighborhoods that experienced the highest levels of storm surge flooding from Katrina. Although Class 4 (built-up loss) has been identified, the size difference between Class 4 (1.96 km^2) and Class 5 (approximately 50 times larger) indicates that permanent abandonment of urban land is relatively

small compared to ultimate recovery of housing stock in the study area over the past 20 years; this finding supports Fussell's (2015) conclusion regarding long term population recovery in New Orleans.

4.6. Pre-Transition Land Cover of New Built-up Pixels

Overlay analysis of Class 3 trajectory pixels against the 2004 XGBoost baseline classification reveals that Forested Wetland was the overwhelmingly dominant antecedent land cover (Table 8; Figure 8), accounting for 137,767 pixels (123.99 km^2) - 92.8% of all newly built-up areas. Water bodies contributed 5.92 km^2 (4.4%), and Vegetation contributed 3.67 km^2 (2.7%).

Table 8: Pre-transition land cover origins of new built-up pixels (Class 3 trajectory) from 2004 XGBoost baseline classification.

Class	Pre-Transition Cover (2004)	Pixel Count	Area (km^2)	% Total
1	Water	6,578	5.92	4.4%
3	Forested Wetland	137,767	123.99	92.8%
4	Vegetation	4,080	3.67	2.7%
	Total	148,425	133.58	100%

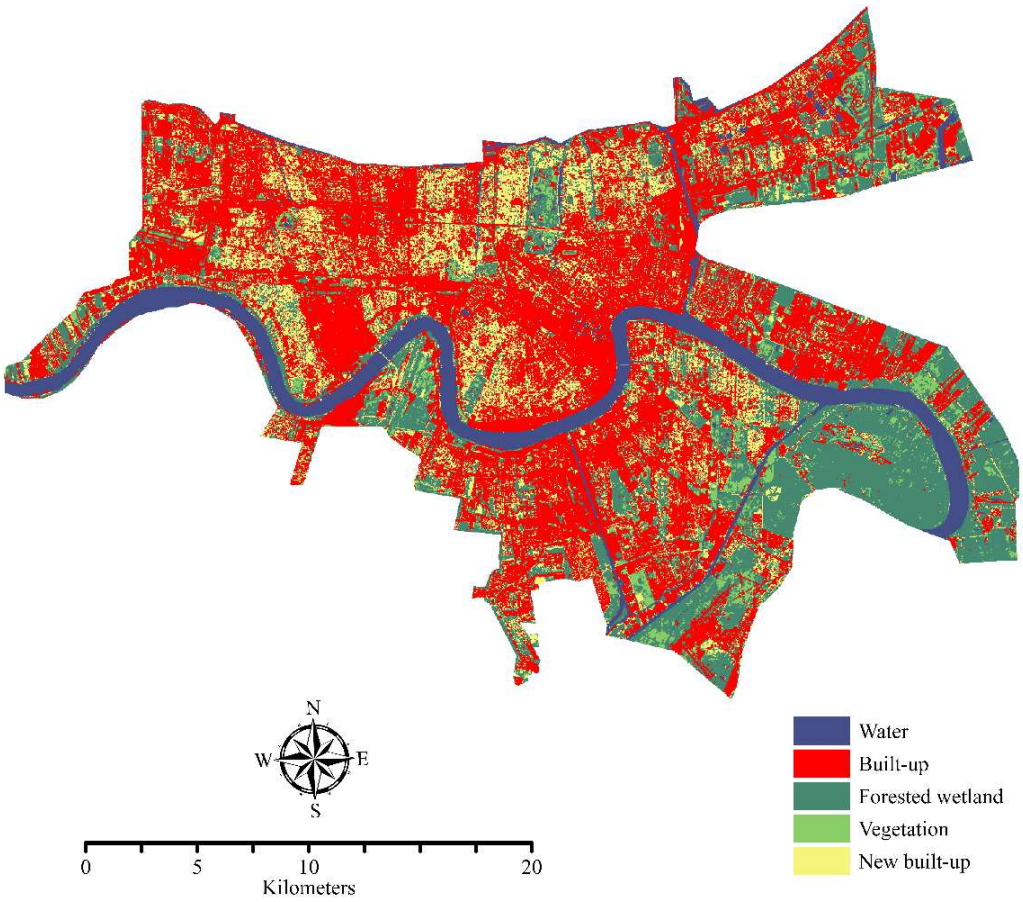


Fig. 8 Pre-transition land cover composition of newly built-up pixels (Class 3) from 2004 XGBoost baseline

Forested wetlands have been converted into built-up land (123.99 km²; 92.8% of total) at an ecologically significant rate. Storm surges are reduced by these areas, as well as their role in capturing CO_2 through carbon sequestration. Additionally, they support fish populations for commercial fishing (Chuang et al. 2019). The scale of the conversion far outpaces replacement of previously developed parcels that were destroyed due to flooding after Hurricane Katrina. Therefore, a considerable amount of "regenerating" of properties has occurred through development in ecological buffer zones and could potentially lead to increased vulnerability to hurricane damage.

4.7. Built-up Loss and Dynamic Categories (Classes 4, 6, 7)

The Built-up loss (Class 4: 1.96 km^2) class represents the smallest size category for a trajectory type and was found to be in areas that were most heavily damaged from the storm in both the Lower Ninth Ward and New Orleans East. Additionally, as residential demolition continues through Compulsory Buy Out programs, as well as due to long-term post-storm vacancy, this has hindered the ability of urban land to recover over the course of the entire study period. While Class 4 represented the smallest total areal extent among all of the classes examined, it also represents an extreme example of how race influences the geography of disinvestment, which occurred after Katrina, as described in (Kamel 2012) and (Lewis et al. 2017). Fluctuating Built-up (Class 6: 44.79 km^2) trajectories are primarily occurring along the urban-wetland fringe in eastern New Orleans and coastal Plaquemines Parish. This reflects instability on marginally productive lands; cyclical speculation in new developments; and ambiguity in spectral classification for transitioning from built to non-built status. Finally, Other Dynamic Non-Built (Class 7: 153.50 km^2) represents dynamic processes within ecological systems that continue today and occur throughout much of the southern and eastern portions of the watershed dominated by wetlands.

4.8. Spatial Autocorrelation of Trajectory Classes

Global Moran's I was statistically significant ($p < 0.001$, 999 permutations) for all seven trajectory classes, confirming that the spatial patterns described in Sections 4.5 and 4.6 are non-random and represent genuine neighborhood-scale clustering of regeneration outcomes across the Greater New Orleans study area (Table 9; Figure 9).

Table 9: Global Moran's I result for all seven trajectory class proportions at the census tract scale (queen contiguity weights, row-standardized; 999 permutations). All classes are significant at $p < 0.001$.

Trajectory Class	Moran's I	E[I]	z-score	p	Sig.	Pattern
Water	0.4134	−0.003	12.97	<0.001	***	Clustered
Stable Built-up	0.5015	−0.003	15.71	<0.001	***	Clustered

New Built-up / Regeneration	0.4810	−0.003	15.08	<0.001	***	Clustered
Built-up Loss	0.1355	−0.003	4.31	<0.001	***	Clustered
Decline then Recovery	0.5121	−0.003	16.05	<0.001	***	Clustered
Fluctuating Built-up	0.3419	−0.003	10.74	<0.001	***	Clustered
Other Dynamic Non-Built	0.5450	−0.003	17.07	<0.001	***	Clustered

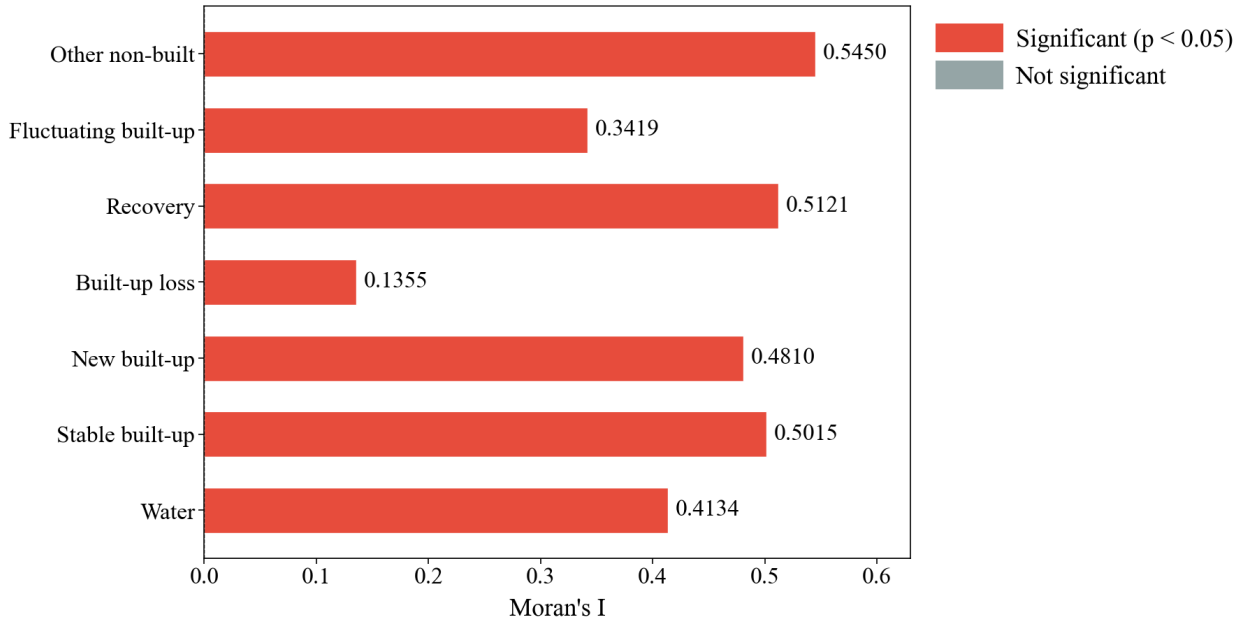


Fig. 9 Global Moran's *I* value for all seven trajectory classes at census tract scale ($p < 0.001$ for all, 999 permutations)

The strongest Moran's I values were observed for Other Dynamic Non-Built (Moran's I = 0.545; z = 17.07); Decline then Recovery (Moran's I = 0.512; z = 16.05); and Stable Built-up (Moran's I = 0.502; z = 15.71). A high degree of spatial autocorrelation of Other Dynamic Non-Built is expected due to the geographic contiguity of the forested wetland and open water body areas along the southeast coastal margin. Spatially organized neighborhood-scale waves are evident from the clustering observed for the Decline then Recovery trajectory (Moran's I = 0.512): this indicates that post-disaster regeneration does not occur as a scattered event at each individual parcel but rather occurs in clusters of parcels within neighborhoods. This pattern supports the tipping point, as identified by (Olshansky et al. 2008), based on neighborhood-level behavior.

Built-up Loss was associated with the lowest Moran's I value for any trajectory type (Moran's I = 0.136; z = 4.31), indicating that, while there may be statistical clustering of permanently abandoned parcels, these parcels appear to be much more dispersed than those experiencing recovery. These findings suggest an asymmetric relationship between the two types of trajectories -- clustering is observed among recovery trajectories (e.g., federal grant-funded recoveries, homeowner social networks, proximity to working infrastructure) and weaker or no clustering is observed among permanent loss trajectories (e.g., individual parcel buyouts, insecure tenures, demolitions). The LISA Decomposition Method found that there is statistical significance for clustering and outliers for each of the seven Trajectory Classes (Table 10; Figure 10).

There are 39 High-High (HH) hot-spot tracts and 62 Low-Low (LL) cold-spot tracts in Decline then Recovery Class. HH tracts (high recovery tracts that have their neighbors also at high recovery) tend to be located near one another in the following neighborhoods: Gentilly, Lakeview, Broadmoor, and Chalmette. These areas constitute a contiguous recovery corridor on both sides of an elevated levee ridge. On the other hand, the LL tracts (low recovery tracts surrounded by low recovery tracts) are primarily found in the Lower Ninth Ward, New Orleans East, and Coastal Plaquemines Parish. Geographical locations of these areas correspond to those characterized by long-term vacancy rates and lower return rates than the rest of the city, as well as negative ΔUII values. Spatial correspondence between the LISA Cold Spots and the Persistent Vacancy neighborhood cluster (Cluster 3) from the K-Means Analysis (Section 4.9) provides convergent validation through two distinct analytical methods.

In the Stable Built-up class, there are 43 HH tracts that form a cohesive band along the Mississippi River Levee Corridor in Uptown, Garden District, CBD, and Metairie, thus validating the levee corridor as the most resilient part of the city's metropolitan area. In the New Built-

605 up/Regeneration Class (I = .481), there are 42 HH and 68 LL tracts. The presence of LL cold spots
606 in the center of the bowl confirms that true new built-up development and regeneration occurred
607 only in the elevated suburbs. The Other Dynamic Non-Built Class contains the highest number of
608 LL Tracts of any of the classes (91 tracts), which reflects the spatial distribution of Wetland Census
609 Tract areas within coastal Plaquemines and St. Bernard Parishes.

610 **Table 10**: LISA cluster counts by trajectory class. HH = High-High (hot spot); LL = Low-Low
611 (cold spot); HL/LH = spatial outliers. Total census tracts, n = 332. Significance at $p < 0.05$ (999
612 permutations).

Trajectory Class	HH	LL	HL	LH	Not Significant
Water	29	48	0	7	248
Stable Built-up	43	48	7	5	229
New Built-up / Regeneration	42	68	1	9	212
Built-up Loss	14	41	3	9	265
Decline then Recovery	39	62	4	4	223
Fluctuating Built-up	28	51	9	5	239
Other Dynamic Non-Built	47	91	0	5	189

613

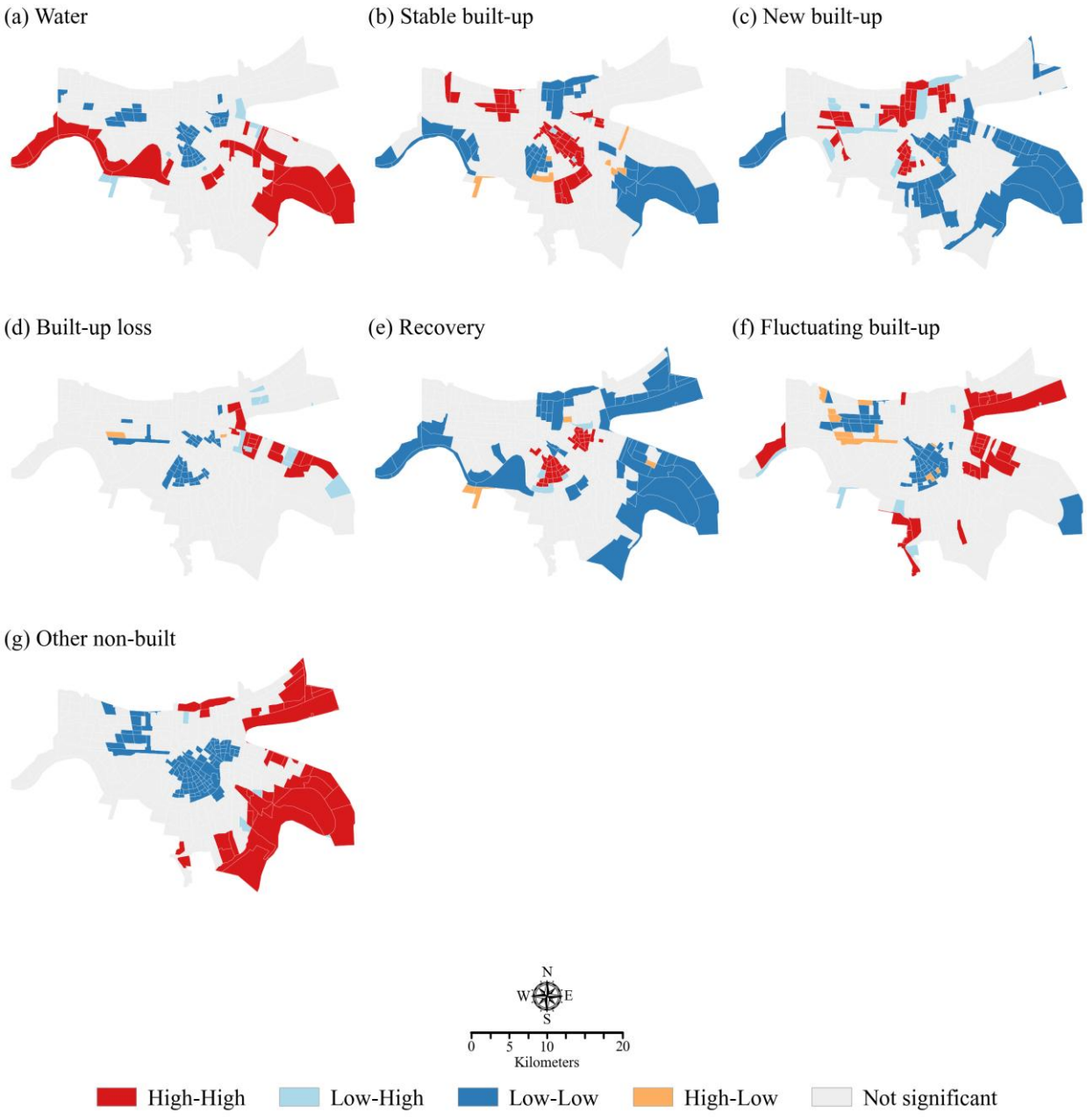


Fig. 10 LISA cluster maps for all seven temporal trajectory classes, Greater New Orleans census tracts

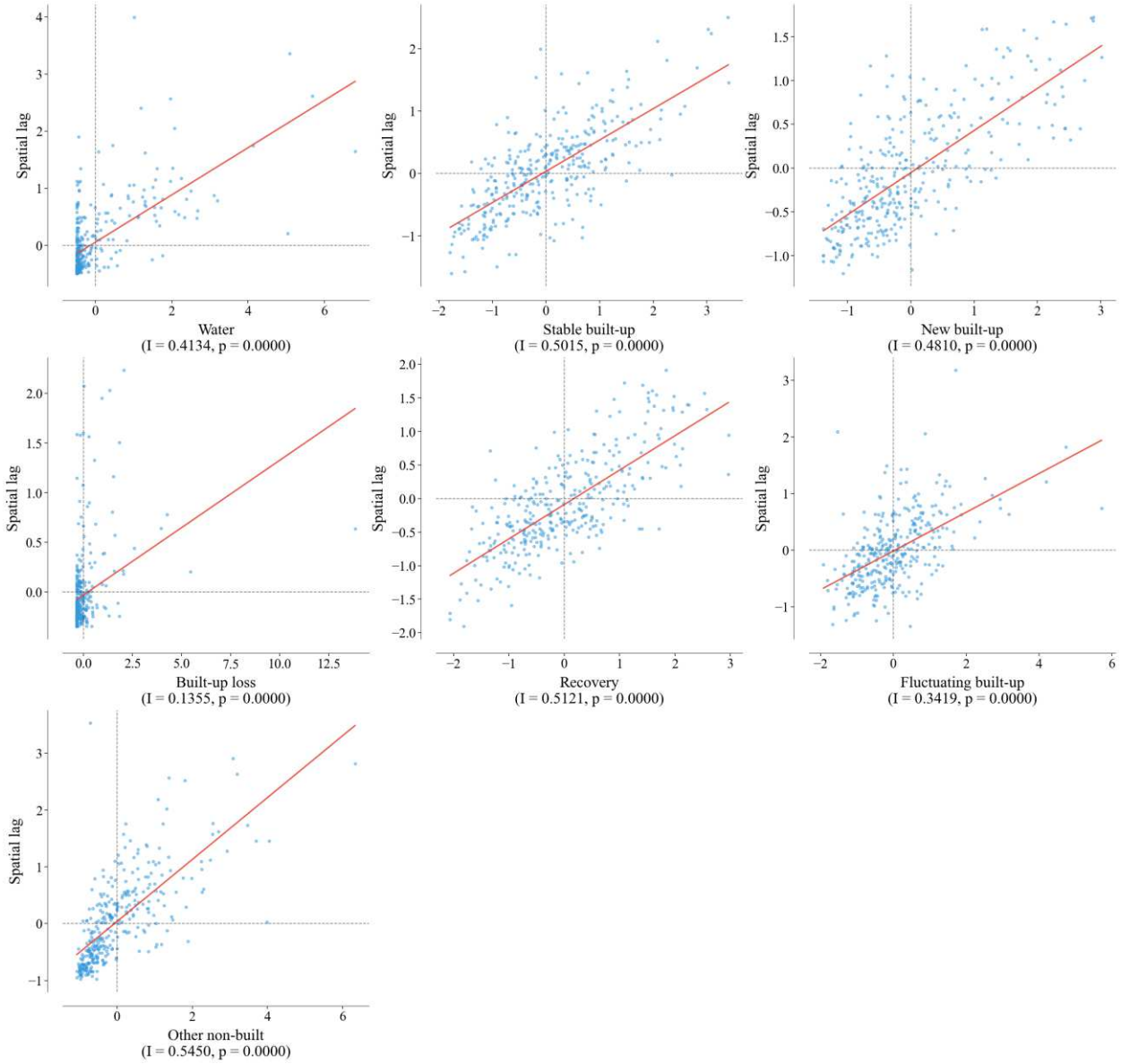


Fig. 11 Moran scatter plots for all seven trajectory classes. The slope of the OLS regression line equals Moran's I. All relationships are positive and significant ($p < 0.001$)

4.9. Neighborhood Typology Clustering

The K-Means clustering identified an optimal K = 4 based on the convergent Elbow, and Silhouette criteria (Figure 2), resulting in four neighborhood archetypes that correspond with the socioeconomic and environmental gradients of Katrina flood impacts documented in the recovery literature (Kamel 2012; Qiang and Lam 2016; Fraser et al. 2022). Cluster profiles are summarized in Table 11 and are shown in Figure 12.

Table 11: Four-cluster neighborhood typology summary with LISA correspondence. LISA tracts from Table 10.

Cluster	Label	Defining Characteristics and LISA Correspondence
1	Resilient Urban Core	High elevation (>1.5 m MSL), dominant Class 2 trajectory, highest mean ΔUII. Corresponds to 43 LISA HH Stable Built-up tracts along the elevated levee ridge: French Quarter, Garden District, Uptown, Metairie.
2	Regeneration Hotspot	Low-moderate elevation, high Class 5 and Class 3 proportions, significant Road Home / CDBG-DR receipt. Corresponds to 39 LISA HH Decline then Recovery tracts: Gentilly, Lakeview, Broadmoor, Chalmette.
3	Persistent Vacancy	Low elevation, high Class 4 and Class 6 proportions, high post-storm vacancy, low population return, and lowest mean ΔUII. Corresponds to 62 LISA LL Decline then Recovery tracts: Lower Ninth Ward, New Orleans East, parts of St. Bernard.
4	Chronic Decline	Very low to low elevation, low OSM road and building density, dominant Class 7 trajectories, negligible ΔUII, minimal post-storm reconstruction activity. Encompasses both outer suburban fringe tracts experiencing land-use contraction (suburban Jefferson, St. Charles) and coastal-margin tracts with sustained wetland encroachment (Plaquemines, St. Bernard). Corresponds to 68 LISA LL New Built-up and 47 LISA HH / 91 LISA LL Other Non-Built tracts where built environment has not recovered to pre-storm extent.

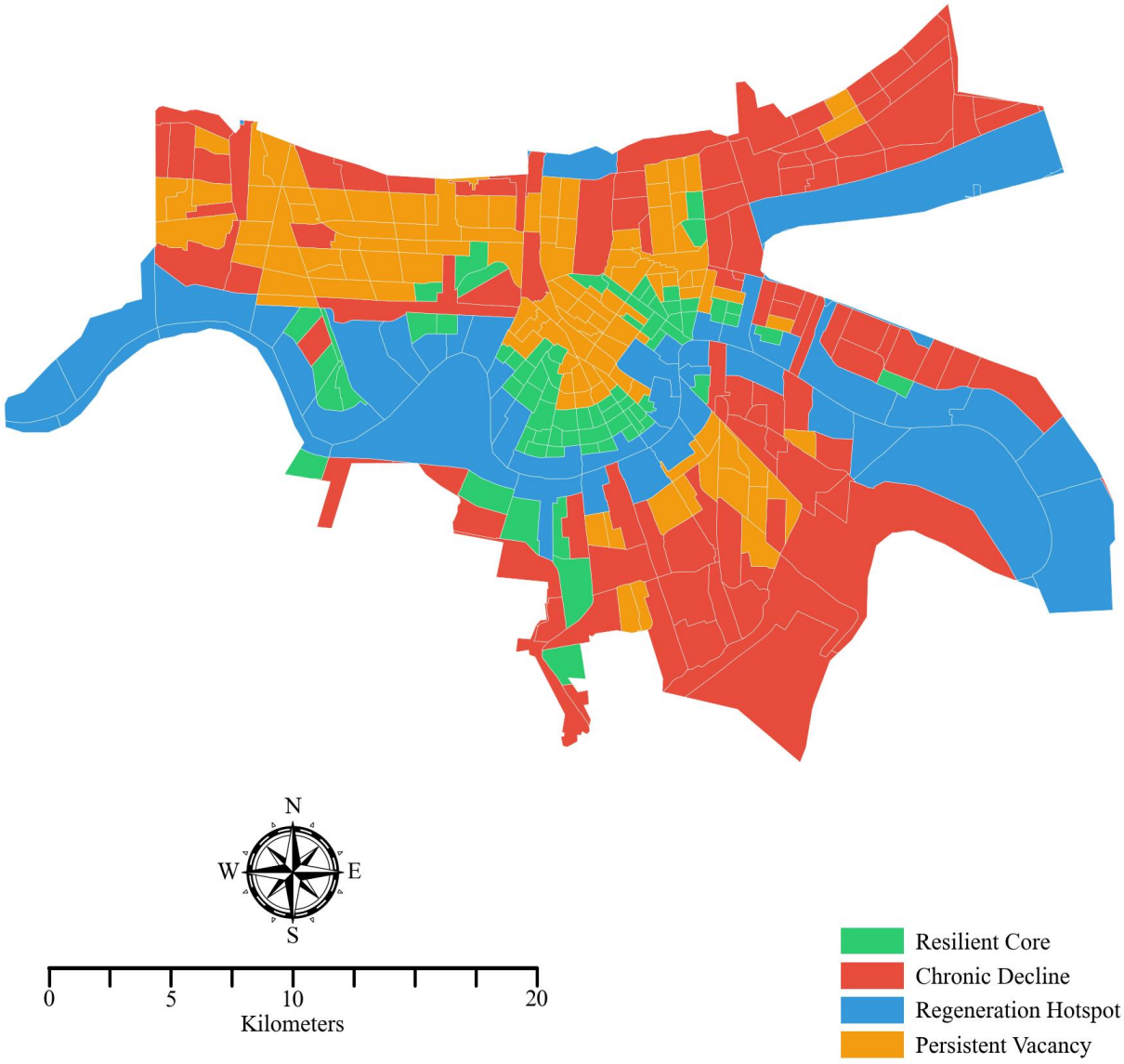


Fig. 12 Neighborhood typology cluster map, Greater New Orleans

The ring-shaped distribution of clusters: Resilient Urban Core on the high ground of the levee, Regeneration Hotspots surrounding it, Persistent Vacancy in the low areas within, and Chronic Decline in the outer parishes and on the coastal margin, illustrating how elevation, flood risk and socio-economic status have been known to determine the nature of disaster recovery (Kamel 2012; Qiang and Lam 2016; Fraser et al. 2022). The above-described pattern of concentrically distributed clusters has also been demonstrated by the LISA analysis as follows.

First, the statistically verified ring-shaped spatial gradients of decline and recovery reflect the locations of HH hot spots for Decline, then Recovery, and Stable Built-up. Second, these statistically verified ring-shaped spatial gradients of decline and recovery correspond to the locations of LL cold spots for both classes. Third, therefore, the statistically verified ring-shaped spatial gradients of decline and recovery match exactly the previously described typology of clusters.

5. Discussion

5.1. The Geography of Recovery: Elevation and Trajectory Outcomes

Spatial variations in trajectory types or neighborhood cluster patterns indicate how post-Katrina recovery in greater New Orleans was influenced by a combination of physical vulnerabilities as well as socio-economic resources. Cluster 1, which is identified as the Resilient Urban Core, includes areas that are characterized by having stable built-up (stable number of buildings within a specific area) and high ΔUII (a measure of urban surface intensity) due to higher elevations and dense OSM building coverages near major roads. Conversely, Cluster 3, which represents the Persistent Vacancy cluster, includes areas with lower elevation levels, sparse OSM building densities, and higher shares of Built-up Loss (Class 4) and Fluctuating Built-up (Class 6) and the lowest mean ΔUII. These spatial distributions are consistent with previous studies examining the racialized nature of recovery in the greater New Orleans area (Kamel 2012; Fussell 2015; Lewis et al. 2017).

This remote sensing-based trajectory analysis provides additional detail regarding the previously found recovery gradient by providing spatial details of the gradient using a 30m-resolution image captured over approximately 20 years. Moreover, the trajectory data also provided a method for conducting statistical analyses (spatial autocorrelation) on the results.

Statistical analysis conducted in this study used Moran's I to examine the degree to which recovery in Greater New Orleans occurred in a clustered fashion versus random events. A Moran's I value > 0 indicates positive spatial autocorrelation, suggesting that recovery is occurring in similar ways throughout an area. The Moran's I statistic indicated that the Decline then Recovery class had an I-value of 0.512, and the Built-up Loss had an I-value of 0.136.

Therefore, the results suggest that while permanent loss is far less clustered than recovery, recovery occurs primarily in a clustered manner at the neighborhood level. Neighborhood tipping point theory (Olshansky et al. 2008) supports these findings as it suggests that once neighboring properties begin to recover, other nearby property owners will be motivated to do likewise, creating recovery "corridors" based upon geographic proximity. Additionally, permanent loss is likely caused by individual homeowner decision-making and/or programmatic eligibility for demolition/vacancy, therefore creating more random patterns compared to recovery patterns. Thus, there are important implications for policymakers as they consider how best to support recovery efforts. For example, investments made into larger-scale neighborhood-wide initiatives such as coordinated rebuilding incentives or anchor institutions could potentially provide more bang-for-buck relative to smaller-scale parcel-based incentive programs since they would take advantage of pre-existing spatial clustering associated with recovery processes.

Finally, the fact that Class 5 (Decline then Recovery) was found to exceed Class 4 (Built-up Loss) by nearly a factor of 50 at the metropolitan scale contradicts narratives suggesting long-term urban decline. However, the 62 LISA Low-Low (LL) recovery cold spots located in the Lower Ninth Ward and New Orleans East demonstrate that although permanent disinvestment is geographically limited to certain neighborhoods, it is still socially concentrated among communities that face significant structural obstacles to recovery. Metropolitan-scale metrics

mask both successful regeneration efforts in more resilient areas of the city and severe permanent disinvestment efforts in the most vulnerable areas of the city.

5.2. SHAP Interpretability: What the Classifier Learned About Katrina

The SHAP analysis is much more than a methodological validation procedure; it provides evidence of an important aspect of the spectral history of the catastrophic event itself. The dominance of the BLUE band in 2005 (mean |SHAP| = 0.88), a spectral measure of standing floodwaters, was a simultaneous occurrence on the order of hundreds of thousands of pixels across the entire study area. The model thus clearly demonstrated that blue reflectance, and specifically its elevation compared to NIR, were the two most discriminating spectral signals present immediately after the inundation. Importantly, it did so based upon features automatically extracted by the classifier, as opposed to being assumed beforehand.

In addition to tracking standing surface waters, the SHAP analysis also shows how the MNDWI index increased during the recovery process (2009: 0.33; 2021: 0.48). These changes represent another type of physical phenomenon related to recovery, namely, persistent soils saturated with water and/or shallow water tables found in areas experiencing slow drainage or limited reconstruction. Field observations from both New Orleans East and the Lower Ninth Ward provide support for these findings, which include prolonged soil waterlogging due to post-storm degradation of drainage infrastructure over many years. Lastly, the significant increase in SHAP value for NIR in 2025 (|SHAP| = 1.10) can be interpreted as indicative of the advanced stage of development of the post-Katrina landscape after two decades of wetland succession and regeneration of forest and suburban vegetation.

Notably, SHAP values for NDBI remain very low throughout all seven epochs (maximum of 0.092), even though NDBI is one of two terms used in the UII equation that should have some

degree of positivity. In the coastal deltaic environment of this study site, significantly more discriminatory spectral information has been found in SWIR1, NIR, and MNDWI when identifying constructed surfaces than in NBDI in any time frame. As such, there appears to be a strong rationale for reconsideration and possible revision of the UII equation that would replace or augment NBDI with either MNDWI or SWIR1 as the built-up component, thereby creating an additional opportunity for developing a new "urban-intensity" metric that is more representative of a geographically specific coastal environment.

5.3. The Ecological Cost of Regeneration: Wetland Conversion

The fact that 92.8 percent of new "built-up" area growth (Class 3) was derived from "forested wetland" in 2004 is the most environmentally relevant outcome of this study. The authors suggest two processes are operating concurrently. First, actual land use change: as documented qualitatively by (Chuang et al. 2019) and Couvillion et al. (2017) post-Katrina suburban expansion in Jefferson and St. Charles parishes displaced urban residents from their homes due to damage from flooding, thus creating a large-scale extension of pre-existing developed areas into previously undeveloped wetland fringe zones. Second, a process of misclassification is based on changes in spectral reflectance caused by the drying of forested wetlands after they were inundated. Field verification of the mechanism(s) responsible for this change will require parcel-level building permits and/or other means of determining whether the wetlands were converted for development purposes.

The results of the LISA analysis add to the environmental concerns discussed above. Specifically, the 68 Low-Low (LL) cold spots identified using LISA within the Suburban Expansion zone surrounding the urban recovery core represent tracts that have undergone little regeneration. Additionally, these tracts are located near tracts classified as low-regeneration

wetland periphery tracts; therefore, it appears there has been a limited amount of urban renewal activity adjacent to the recovery core. These findings support a green-field model of urbanization rather than an infill regeneration model and indicate that the loss of wetland function is being driven primarily through loss of natural vegetation cover rather than through subsequent spectral artifacts resulting from parcels that were once flooded but are now dry.

5.4. Limitations of the Study

This study has several limitations. First, the footprint layer reflects present-day building locations, it does not capture structures that existed in 2005 but were later demolished, nor does it exclude structures built after 2005. ΔUII therefore measures change in surface intensity at present-day building locations, not change in the extent of the built environment, which is captured separately by the trajectory analysis. Second, the 5 km spatial block size used for cross-validation was chosen based on practical considerations rather than testing sensitivity to different block sizes. Finally, we specified queen-contiguity as the weight option for Moran's I, but other options are available, and we did not test how different specifications would affect our results.

6. Conclusions

This study contributes to the literature on post-disaster remote sensing research through four major methodological improvements. First, this study represents, to the authors' knowledge, the longest single continuous satellite monitoring of an individual US disaster recovery. Second, it addresses a systematic overconfidence bias in many remote-sensing studies (Roberts et al. 2017) by utilizing spatially split cross-validation. Third, the application of SHAP values allows for an interpretable and detailed examination of which features are most important at each stage of the disaster event - an application of SHAP that has never been applied before in the literature of post-disaster remote sensing. Lastly, combining Global Moran's I, LISA, and K-Means clustering

techniques yields spatial evidence for socioeconomic stratification of recovery that cannot be obtained from these methods individually.

The first major conclusion from this study is that the footprint-level recovery of the entire metropolitan area of Greater New Orleans is virtually complete. There was a total of 97.88 km^2 of the decline, then recovery trajectory. That number exceeds the permanent loss of built-up land cover of 1.96 km^2. This is significant because it challenges some common narratives about urban shrinkage and permanent loss of developed land. However, to be clear, the recovery that occurred thereafter was primarily in elevated, relatively affluent areas. The second major conclusion is that the post-Katrina regeneration of New Orleans is organized by neighborhoods at a scale much larger than individual parcels. Global Moran's I confirmed that there is indeed neighborhood-scale spatial organization to the post-disaster regeneration of the city (Global Moran's I=0.512, z=16.05, $p<0.001$). These results are also supported by Local Indicators of Spatial Association (LISA), which found 39 HH recovery hotspots forming a coherent corridor in Gentilly, Lakeview, and Broadmoor. Conversely, LISA identified 62 LL coldspots located in both the Lower Ninth Ward and New Orleans East. Therefore, these statistically confirmed spatial patterns provide strong evidence for an equity narrative that has been documented in qualitative form in the social science literature. Third, the post-disaster recovery of New Orleans exhibited a spatial stratification that mirrored and reinforced existing socioeconomic inequalities.

There are four distinct neighborhood archetypes: Chronic decline, Persistent vacancy, Regeneration hotspot, and Resilient Urban Core. The LISA identified three of those corresponding to pre- and post-hurricane socioeconomic status: Affluent/Regeneration Hotspot; Working Class/Resilient Urban Core; Low Income/Persistent Vacancy. While the working-class/resilient urban core archetype had the highest proportion of its original residents returned by the end of

2018, it still had lower rates of resident return than similar cities. Furthermore, many of the neighborhoods classified under this archetype experienced greater levels of vacant housing during this period. The Persistent Vacancy archetype corresponds to those neighborhoods where less than half of their original residents returned by the end of 2018. It is characterized by a negative mean ΔUII, high vacancy rates, and very low population return, despite nearly two decades of federally funded investments in this area. Fourth, the new built-up development associated with post-disaster urban growth resulted in a large ecological impact. In fact, approximately 92.8 percent of the new built-up development (123.99 km^2) was converted from land that was forested wetland in 2004. As such, coastal habitats that previously served as buffers against storms now act as impervious surfaces, potentially exacerbating flooding. The LISA analysis of the New Built-up class further supports concerns regarding this trend: LL cold spots in the suburban expansion areas indicate that this type of development is spatially segregated from the urban recovery core and therefore likely represents a true greenfield conversion rather than urban infill regeneration. Fifth, SHAP value decomposition provided a physically meaningful spectral representation of the disaster event itself: Dominance of the BLUE band in 2005 (mean |SHAP|=0.88) indicates the presence of standing water throughout the city after Katrina; elevation increase in MNDWI throughout the epochs of recovery indicates continued soil saturation; and re-emergence of NIR in 2025 (|SHAP|=1.10) indicates two decades of wetland canopy maturation. Lastly, the consistently low SHAP values assigned to NDBI across all epochs indicate that this index should be used with caution when classifying coastal deltaic urban landscapes using remotely sensed data, due to its limited sensitivity to changes in vegetation cover in saturated soils.

References

Anselin L (1995) Local Indicators of Spatial Association—LISA. Geogr Anal 27:93–115. https://doi.org/10.1111/j.1538-4632.1995.tb00338.x

Aune KT, Gesch D, Smith GS (2020) A spatial analysis of climate gentrification in Orleans Parish, Louisiana post-Hurricane Katrina. Environ Res 185:109384. https://doi.org/10.1016/j.envres.2020.109384

Belgiu M, Drăguţ L (2016) Random forest in remote sensing: A review of applications and future directions. ISPRS J Photogramm Remote Sens 114:24–31. https://doi.org/10.1016/j.isprsjprs.2016.01.011

Breiman L (2001) Random Forests. Mach Learn 45:5–32. https://doi.org/10.1023/A:1010933404324

Chastain R, Housman I, Goldstein J, et al (2019) Empirical cross sensor comparison of Sentinel-2A and 2B MSI, Landsat-8 OLI, and Landsat-7 ETM+ top of atmosphere spectral characteristics over the conterminous United States. Remote Sens Environ 221:274–285. https://doi.org/10.1016/j.rse.2018.11.012

Chen T, Guestrin C (2016) XGBoost: A Scalable Tree Boosting System. In: Proceedings of the 22nd ACM SIGKDD International Conference on Knowledge Discovery and Data Mining. ACM, San Francisco California USA, pp 785–794

Chuang W-C, Eason T, Garmestani A, Roberts C (2019) Impact of Hurricane Katrina on the Coastal Systems of Southern Louisiana. Front Environ Sci 7:. https://doi.org/10.3389/fenvs.2019.00068

Composto RW, Tulbure MG, Tiwari V, et al (2025) Quantifying urban flood extent using satellite imagery and machine learning. Nat Hazards 121:175–199. https://doi.org/10.1007/s11069-024-06817-5

Couvillion BR, Beck H, Schoolmaster D, Fischer M (2017) Land area change in coastal Louisiana (1932 to 2016). U.S. Geological Survey

Dronova I, Gong P, Clinton NE, et al (2012) Landscape analysis of wetland plant functional types: The effects of image segmentation scale, vegetation classes and classification methods. Remote Sens Environ 127:357–369. https://doi.org/10.1016/j.rse.2012.09.018

Fraser T, Poniatowski AR, Hersey N, et al (2022) Uneven paths: Soft Policy's benefits to recovery in Louisiana Parishes after Hurricanes Katrina and Rita. J Environ Manage 321:115722. https://doi.org/10.1016/j.jenvman.2022.115722

Fussell E (2015) The Long Term Recovery of New Orleans' Population after Hurricane Katrina. Am Behav Sci 59:1231–1245. https://doi.org/10.1177/0002764215591181

Fussell E, Curtis KJ, DeWaard J (2014) Recovery Migration to the City of New Orleans after Hurricane Katrina: A Migration Systems Approach. Popul Environ 35:305–322. https://doi.org/10.1007/s11111-014-0204-5

Gorelick N, Hancher M, Dixon M, et al (2017) Google Earth Engine: Planetary-scale geospatial analysis for everyone. Remote Sens Environ 202:18–27. https://doi.org/10.1016/j.rse.2017.06.031

Gotham KF, Campanella R (2011) Coupled Vulnerability and Resilience: the Dynamics of Cross-Scale Interactions in Post-Katrina New Orleans. Ecol Soc 16:art12. https://doi.org/10.5751/ES-04292-160312

Gotham KF, Greenberg M (2008) From 9/11 to 8/29: Post-Disaster Recovery and Rebuilding in New York and New Orleans. Soc Forces 87:1039–1062

Homeland Security, Federal Emergency Management Administration (FEMA) (2006) Hurricane Katrina in the Gulf Coast: building performance observations, recommendations, and technical guidance. Mitigation Assessment Team Report, FEMA 549. U.S.

Kamel N (2012) Social Marginalisation, Federal Assistance and Repopulation Patterns in the New Orleans Metropolitan Area following Hurricane Katrina. Urban Stud 49:3211–3231. https://doi.org/10.1177/0042098011433490

Kates RW, Colten CE, Laska S, Leatherman SP (2006) Reconstruction of New Orleans after Hurricane Katrina: a research perspective. Proc Natl Acad Sci U S A 103:14653–14660. https://doi.org/10.1073/pnas.0605726103

Kondo T (2017a) Spatial Characteristics and Impact on Built Environment Regeneration by Property Transfer and Regeneration Programs After Hurricane Katrina. J Archit Plan Trans AIJ 82:715–722. https://doi.org/10.3130/aija.82.715

Kondo T (2017b) LONG-TERM CHANGE OF POST-DISASTER HOUSING RECOVERY AND EFFECTIVENESS OF PROPERTY TRANSFER AND REGENERATION PROGRAMS BY LOCAL GOVERNMENT A study on housing rebuilding in City of New Orleans after Hurricane Katrina (2005). J Archit Plan Trans AIJ 82:1511–1520. https://doi.org/10.3130/aija.82.1511

Lewis J, Zipperer W, Ernstson H, et al (2017) Socioecological Disparities in New Orleans Following Hurricane Katrina. Ecosphere 8:. https://doi.org/10.1002/ecs2.1922

Lin L, Di L, Zhang C, et al (2024) Modeling urban redevelopment: A novel approach using time-series remote sensing data and machine learning. Geogr Sustain 5:211–219. https://doi.org/10.1016/j.geosus.2024.02.001

Lundberg S, Lee S-I (2017) A Unified Approach to Interpreting Model Predictions

Lundberg SM, Erion G, Chen H, et al (2020) From Local Explanations to Global Understanding with Explainable AI for Trees. Nat Mach Intell 2:56–67. https://doi.org/10.1038/s42256-019-0138-9

Maxwell A, Warner T, Fang F (2018) Implementation of machine-learning classification in remote sensing: An applied review. Int J Remote Sens 39:2784–2817. https://doi.org/10.1080/01431161.2018.1433343

Miller AJ, Arias ME, Alvarez S (2021) Built environment and agricultural value at risk from Hurricane Irma flooding in Florida (USA). Nat Hazards 109:1327–1348. https://doi.org/10.1007/s11069-021-04880-w

Olshansky RB, Johnson LA, Horne J, Nee B (2008) Longer View: Planning for the Rebuilding of New Orleans. J Am Plann Assoc 74:273–287. https://doi.org/10.1080/01944360802140835

Qiang Y, Lam N (2016) The impact of Hurricane Katrina on urban growth in Louisiana: an analysis using data mining and simulation approaches. Int J Geogr Inf Sci 30:1–21. https://doi.org/10.1080/13658816.2016.1144886

Roberts DR, Bahn V, Ciuti S, et al (2017) Cross-validation strategies for data with temporal, spatial, hierarchical, or phylogenetic structure. Ecography 40:913–929. https://doi.org/10.1111/ecog.02881

Rousseeuw PJ (1987) Silhouettes: A graphical aid to the interpretation and validation of cluster analysis. J Comput Appl Math 20:53–65. https://doi.org/10.1016/0377-0427(87)90125-7

Scoppetta C (2016) “Natural” disasters as (neo-liberal) opportunity? Discussing post-hurricane Katrina urban regeneration in New Orleans. TeMA J Land Use Mobil Environ 9:. https://doi.org/10.6092/1970-9870/3725

U.S. Department of Housing and Urban Development (2007) Federal Register 72(237):70472–70474 (Docket No. FR–5183–N–01)

Valavi R, Elith J, Lahoz-Monfort JJ, Guillera-Arroita G (2018) blockCV: an R package for generating spatially or environmentally separated folds for k-fold cross-validation of species distribution models. 357798

van Holm EJ, Wyczalkowski C (2018) Gentrification in the wake of a hurricane: New Orleans after Katrina. Urban Stud 56:004209801880044. https://doi.org/10.1177/0042098018800445

Wang Q, Gu H, Zang X, et al (2025) Flood resilience in cities and urban agglomerations: a systematic review of hazard causes, assessment frameworks, and recovery strategies based on LLM tools. Nat Hazards 121:12391–12426. https://doi.org/10.1007/s11069-025-07285-1

Weng Q, Lu D, Schubring J (2004) Estimation of land surface temperature–vegetation abundance relationship for urban heat island studies. Remote Sens Environ 89:467–483. https://doi.org/10.1016/j.rse.2003.11.005

Xu H (2008) A new index for delineating built-up land features in satellite imagery. Int J Remote Sens 29:4269–4276. https://doi.org/10.1080/01431160802039957

Zhao C, Qin C-Z (2019) Mapping large-area tidal flats without the dependence on tidal elevations: A case study of Southern China. ISPRS J Photogramm Remote Sens 159:256–270. https://doi.org/10.1016/j.isprsjprs.2019.11.022

Statements and Declarations

Funding The authors have no competing interests to declare that are relevant to the content of this article.

Competing Interests The authors declare that they have no known competing financial interests or personal relationships that could have appeared to influence the work reported in this paper.

Author Contributions Stanley Ejike Osondu: Writing – original draft, Software, Methodology, Investigation, Formal analysis. Muhammad Tauhidur Rahman, Ph.D: Conceptualization, Validation, Visualization, Writing – review & editing, Supervision.

Data availability Building footprint data for the United States are available from the Microsoft US Building Footprints repository. Supplementary building footprint data are available from Neilsberg (https://www.neilsberg.com/research/datasets). U.S. Census tract boundary maps for Louisiana are available from the U.S. Census Bureau (https://www2.census.gov/geo/maps). Additional satellite imagery and derived geospatial datasets used in the Hurricane Katrina analysis are available from their respective data providers. Additional data will be made available on request.

Ethics approval: Not applicable

Consent: Not applicable